

6-26-2015

# Investigation of indentation derived creep response using constant load and constant strain rate methods

Nicholas J. Martinez

Follow this and additional works at: [https://digitalrepository.unm.edu/me\\_etds](https://digitalrepository.unm.edu/me_etds)

---

## Recommended Citation

Martinez, Nicholas J.. "Investigation of indentation derived creep response using constant load and constant strain rate methods." (2015). [https://digitalrepository.unm.edu/me\\_etds/33](https://digitalrepository.unm.edu/me_etds/33)

This Thesis is brought to you for free and open access by the Engineering ETDs at UNM Digital Repository. It has been accepted for inclusion in Mechanical Engineering ETDs by an authorized administrator of UNM Digital Repository. For more information, please contact [disc@unm.edu](mailto:disc@unm.edu).

Nicholas J Martinez

*Candidate*

Mechanical Engineering

*Department*

This dissertation is approved, and it is acceptable in quality and form for publication:

*Approved by the Dissertation Committee:*

Yu-Lin Shen , Chairperson

Mehran Tehrani

Rafiqul A. Tarefder

**INVESTIGATION OF INDENTATION DERIVED CREEP  
RESPONSE USING CONSTANT LOAD AND CONSTANT  
STRAIN RATE METHODS**

**by**

**NICHOLAS J. MARTINEZ**

**B.S. MECHANICAL, UNIVERSITY OF NEW MEXICO (2012)**

**THESIS**

Submitted in Partial Fulfillment of the  
Requirements for the Degree of

**Master of Science  
Mechanical Engineering**

The University of New Mexico  
Albuquerque, New Mexico

**May 2015**

# **Investigation of Indentation Derived Creep Response Using Constant Load and Constant Strain Rate Methods**

**by**

**Nicholas J. Martinez**

B.S. Mechanical Engineering, University of New Mexico, 2012

M.S. Mechanical Engineering, University of New Mexico, 2015

## **ABSTRACT**

Time dependent plastic deformation in metals can occur at high temperatures. Typically the creep test is conducted to characterize the deformation features; however, the conventional uniaxial power-law creep test may be impractical for small scale materials. Accordingly, instrumented indentation techniques are frequently employed. This study concerns the employment of instrumented indentation to characterize the power-law creep response of metallic materials. Indentation derived creep response using constant load-hold and constant indentation strain rate methods were investigated through systematic numerical finite element analysis of conical indentation. The model system of pure tin (Sn) and Sn-based alloy with known uniaxial power-law creep parameters is used for direct comparison between constant indentation strain rate and constant load-hold methods. It was found that each method accurately yielded the corresponding creep stress exponent ( $n$ ); thus, leading to parallel lines of strain rate versus creep stress on the logarithmic scale. It is evident that the constant indentation strain rate method produced more uniform results. A parametric analysis taking into account a wide range of power-law parameters was conducted for the constant

indentation strain rate method. A unique trend of strain rate ratio between the uniaxial creep test and indentation creep test was identified.

# Table of Contents

<b>Chapter 1: Introduction</b> .....	1
1.1 Introduction .....	2
1.2 Technical Background .....	3
1.3 Methodology.....	6
1.4 Thesis Objective .....	11
<b>Chapter 2: Model Description</b> .....	13
2.1 Material Model .....	14
2.2 Constant Load-Hold Model .....	16
2.3 Constant Indentation Strain Rate Model .....	18
2.4 Mesh Convergence .....	21
<b>Chapter 3: Constant Load-Hold Method</b> .....	26
3.1 Constant Load-Hold Method .....	27
<b>Chapter 4: Constant Indentation Strain Rate Method: Parametric Analysis</b> .....	39
4.1 Constant Indentation Strain Rate Method .....	40
4.2 Parametric Analysis (Constant Strain Rate Method) .....	48
<b>Chapter 5: Conclusions and Suggested Future Work</b> .....	51
5.1 Conclusions .....	52
5.2 Suggested Future Work .....	54
<b>References</b> .....	55
<b>Appendix</b> .....	58
A. Model Methodology Verification .....	59
B. Input File - Constant Indentation Strain Rate Method .....	62
C. Input File – Constant Load-Hold Method.....	81

## List of Figures

<b>Figure 1:</b> Typical creep curve of strain versus time at constant P and T .....	4
<b>Figure 2:</b> (L) Schematic of indentation process (R) Standard load & unload displacement curve .....	6
<b>Figure 3:</b> Experimentally measured steady-state creep response for the four material models considered, per Ref. [24] .....	15
<b>Figure 4:</b> 2-D axisymmetric model schematic (Constant Load-Hold Model Schematic) .....	16
<b>Figure 5:</b> 2-D axisymmetric model schematic (Constant strain-rate model schematic) .....	19
<b>Figure 6:</b> Mesh 1 .....	23
<b>Figure 7:</b> Mesh 2 .....	23
<b>Figure 8:</b> Mesh 3 .....	24
<b>Figure 9:</b> Mesh convergence study.....	24
<b>Figure 10:</b> Simulated (P-h) Load-Depth response of pure Sn at 120°C under two different peak loads.....	28
<b>Figure 11:</b> Contour plots of Von Mises stress for the model Sn at 120 °C, with a peak load of 50µN. Indentation is at (a) the beginning of the holding stage (b) the end of the holding stage (30 hours).....	30
<b>Figure 12:</b> Contour plots of Von Mises stress for the model Sn at 120 °C, with a peak load of 100µN. Indentation is at (a) the beginning of the holding stage (b) the end of the holding stage (30 hours).....	31
<b>Figure 13:</b> Contour plots of Equivalent Creep Strain for the model Sn at 120 °C, with a peak load of 50µN. Indentation is at (a) the beginning of the holding stage (b) the end of the holding stage (30 hours).....	32
<b>Figure 14:</b> Contour plots of Equivalent Creep Strain for the model Sn at 120 °C, with a peak load of 100µN. Indentation is at (a) the beginning of the holding stage (b) the end of the holding stage (30 hours) .....	33
<b>Figure 15:</b> Simulated (h-t) Depth-Time response for pure Sn at 120°C under two different peak loads. Time duration of 30 hours.....	35
<b>Figure 16:</b> Simulated (h-t) Depth-Time response for the four Sn-based material models considered under two different peak loads .....	35
<b>Figure 17:</b> Relationship between indentation strain rate and creep stress, obtained from the indentation modeling .....	38
<b>Figure 18:</b> Simulated load-displacement response of SnAgCu at 25 °C under four different strain rates .....	42

<b>Figure 19:</b> Simulated hardness as a function of displacement for SnAgCu at 25 °C .....	42
<b>Figure 20:</b> Contour plots of equivalent creep strain for SnAgCu at 25 ° C under indentation strain rates of (a) $10^{-4}$ [ $s^{-1}$ ] and (b) $10^{-7}$ [ $s^{-1}$ ].....	43
<b>Figure 21:</b> Contour plots of Von Mises effective stress for SnAgCu at 25 ° C under indentation strain rates of (a) $10^{-4}$ [ $s^{-1}$ ] and (b) $10^{-7}$ [ $s^{-1}$ ].....	44
<b>Figure 22:</b> Relationship between indentation strain rate and creep stress, obtained from the constant indentation strain rate modeling.....	47
<b>Figure 23:</b> Parametric analysis study – Strain rate ratio values as a function of the creep stress exponent (n) and the creep constant (A).....	50
<b>Figure 24:</b> Relationship between indentation strain rate and creep stress, obtained from the experimental data in Ref [29]. $\dot{\epsilon}_i - \sigma$ curves obtained through extraction of experimental data in [29] (solid lines). The dashed line represents the power-law creep relation, based on vertically translating the experimentally derived curve by 0.33.....	61



## List of Tables

<b>Table 1:</b> Material Properties used in the constant load- hold and constant strain-rate model...	14
<b>Table 2:</b> Constant load-hold method – Load step conditions applied to the model.....	18
<b>Table 3:</b> Constant strain-rate method – Model inputs for each load step ensuring constant $\dot{\epsilon}_i$ ..	20
<b>Table 4:</b> Database summary of each mesh .....	21
<b>Table 5:</b> Stress exponent and strain-rate ratio obtained from constant load-hold model.....	38
<b>Table 6:</b> Stress exponent and strain-rate ratio obtained from constant load-hold model.....	47

## **Chapter 1: Introduction**

## 1.1 - Introduction

An instrumented indentation test is a convenient technique for measuring the mechanical properties of a material. More specifically, nano/micro indentation testing is a common method for characterizing a material's mechanical response for sub-scale applications such as: thin films, solder joints, and metallization lines [1, 2]. This technique involves forcing a sharp diamond indenter into the surface of the test material, while measuring the force imposed and the corresponding displacement of the indenter. The advances in instrumentation allow for continuous measure of force and displacement as an indentation is made. Accordingly, the yielded load-displacement data may be used to determine mechanical properties even with minimal indentation depths [1-4].

Instrumented indentation testing may also be utilized to study time dependent plastic deformation in materials, particularly the study of creep behavior [5]. Assessing creep behavior through instrumented indentation is progressively growing due to its impending advantages over the conventional uniaxial creep test. These advantages include small specimen volume, constant stress at constant load, and the capability to characterize local mechanical properties of heterogeneous materials, such as grain boundaries and interfaces [6]. In conjunction with these advantages, assessing creep behavior through instrumented indentation is not as straightforward to analyze and interpret as the more conventional uniaxial creep test [7]. Considering the dynamics of deformation differ between the two creep test methods, correlating the indentation

measurement with uniaxial creep behavior becomes a challenge [1-9]. Accordingly, research aimed to gain insight on the relationship between instrumented indentation and conventional uniaxial creep is of great interest.

## 1.2- Technical Background

Creep is defined as the time-dependent and permanent deformation of materials when subjected to a constant load or stress. Creep is normally an undesirable phenomenon and is often the limiting factor in the lifetime of a part [10]. Deformation results from the consistent stress below the yield strength of the material. The amount of applied stress and its duration can eventually lead to the failure of the given material. Creep is observed in all material types; however, metallic materials display the time-dependent plastic deformation behavior at temperatures greater than  $0.4T_m$ , where  $T_m$  is the absolute melting temperature of that particular material [10-11].

Figure 1 represents a typical creep curve of a metallic material. The resulting creep curve consists of three regions, each of which has its own distinctive stress-time feature. Occurring first is the primary or transient creep region. Per Figure 1, it is observed that the slope of the curve reduces with time; thus, suggesting that the material is experiencing an increase in creep resistance or strain hardening. Note that the instantaneous deformation occurs upon initial loading and is totally elastic. The most well understood stage of creep is secondary creep, also referred to as steady-state creep, and attributes a constant slope. The constancy of creep rate is explained on the basis of a balance between the competing processes of strain hardening (due to

dislocation-dislocation interaction) and recovery (due to climb or cross slip), recovery being the process whereby a material becomes softer and retains its ability to experience deformation. Finally, the tertiary creep region illustrates an acceleration of the rate followed by failure. This failure or rupture is a direct result of microstructural and/or metallurgical changes such as grain boundary separation and/or internal microvoids [10-11].

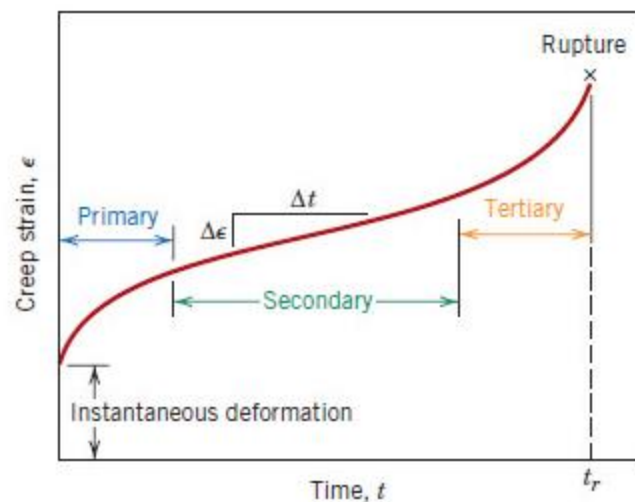


Figure 1: Typical creep curve of strain versus time at constant load and constant elevated temperature

Depending on temperature and applied stress, dislocation glide, dislocation climb, or diffusional flow mechanisms may dominate creep deformation. At high stresses, creep is controlled by the movement of dislocations. Dislocation creep, also termed power-law creep, has a strong dependence on the applied stress and is independent of grain size. The term power-law creep was coined from the simple fact that the creep rate varies with stress to a power greater than unity [12]. The

fundamental mechanism dominating the power-law creep deformation is climb assisted dislocation glide, where the climb is an enabling mechanism allowing dislocations to get around obstacles. Equations specific to the various relaxation mechanisms, including power law-creep and diffusional creep are available.

One of the most important parameters obtained from a creep test is the slope of the secondary (steady-state) region of the creep curve. This is often called the steady-state creep rate,  $\dot{\epsilon}_s$ , and is used as an engineering design parameter. During a conventional uniaxial creep test, a constant axial stress is applied to a bulk specimen. After a short duration, the creep process enters the secondary region; hence, a steady-state relation is achieved where strain rate increases linearly with time [13]. The relationship between steady-state strain rate ( $\dot{\epsilon}_s$ ), applied stress ( $\sigma$ ), and temperature is obtained from the following expression [1-7, 8-13]:

$$\dot{\epsilon}_s = A' \left[ \exp\left(-\frac{Q}{RT}\right) \right] \sigma^n \quad (1)$$

where  $A'$  is a constant,  $n$  is the stress exponent for creep,  $Q$  is the activation energy,  $R$  is the universal gas constant (8.314 J/mol K), and  $T$  is the absolute temperature in Kelvin. At a constant temperature, the steady-state creep rate relation is further simplified per Equation 2.

$$\dot{\epsilon}_s = A\sigma^n \quad (2)$$

where the constants  $A$  and  $n$  uniquely characterize the power-law creep response. The defined power-law creep parameters may be determined by plotting the measured strain rates against the applied stresses, both in the logarithmic scales [10-13]. Uniaxial

tension and compression testing techniques are commonly used to determine these creep response parameters; however, these techniques may be impractical when dealing with materials of small volumes. Accordingly, several instrumented indentation techniques have been investigated in hopes of accurately assessing creep behavior [1-8, 13].

### 1.3 - Methodology

Since its introduction in 1992 by Oliver and Pharr, a powerful method was developed to access the hardness and elastic modulus via instrumented indentation techniques [4]. During an instrumented indentation test, a rigid conical indenter is driven into the materials surface and then retracted under controlled conditions. Examples of these conditions include but are not limited to: load control, displacement history, cyclic (load or displacement), and dwell times at max load.

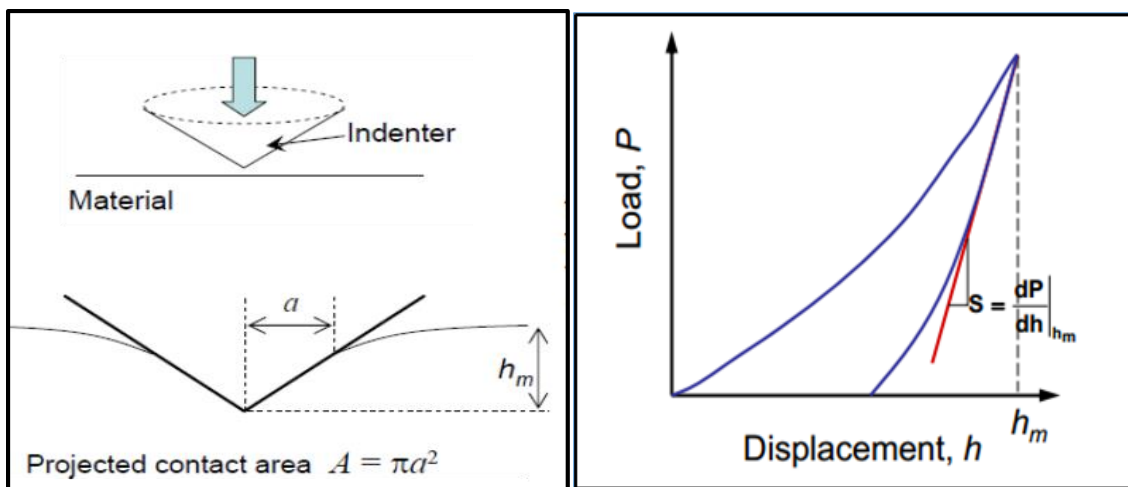


Figure 2: LEFT: Schematic of indentation process. RIGHT: Standard load & unload displacement curve

A typical load-displacement curve during indentation loading and unloading can be seen in Figure 2. During this test procedure, the load (P) and indentation depth (h) are both continuously measured by the indentation testing device. The elastic modulus and hardness of the material is usually obtained according to the Oliver and Pharr method [4]

$$S = \frac{dP}{dh} = \beta \left( \frac{2}{\sqrt{\pi}} \right) E_{eff} \sqrt{A_c} \quad (3)$$

where  $S$  is the contact stiffness defined as the initial slope of the unloading curve, refer to Figure 2.  $\beta$  is a geometry-dependent dimensionless parameter close to unity and accounts for deviations in stiffness caused by lack of symmetry in pyramidal indenters.

$E_{eff}$  is the effective modulus, and  $A_c$  is the projected contact area at the onset of unloading described by the following relation:

$$A_c = \pi a^2 \quad (4)$$

The projected contact area may be approximated as the area projected onto the plane of the original specimen surface per Equation 4. The contact radius,  $a$ , is directly obtained from the field output and is determined by the position of the final node in contact at the onset of unloading. Once the contact stiffness is known, the effective modulus,  $E_{eff}$ , may be obtained per Equation 5.

$$\frac{1}{E_{eff}} = \frac{1-v^2}{E} + \frac{1-v_i^2}{E_i} \quad (5)$$

where  $E_i$ ,  $E$ ,  $v_i$ , and  $v$  are the elastic modulus and Poisson's ratio of the indenter and test material, respectively. The effective elastic modulus takes into account the fact that



elastic displacements occur in both the specimen, with Young's modulus ( $E$ ) and Poisson's ratio ( $\nu$ ), and the indenter, with elastic constants  $E_i$  and  $\nu_i$ . The indentation-derived elastic modulus of the material may then be determined using Equations 3 & 5. The hardness of the material,  $H$ , is directly obtained from:

$$H = \frac{P_{max}}{A_c} \quad (6)$$

where  $P_{max}$  is the maximum applied load [6-13]. The implementation of the general indentation technique, per Oliver-Pharr, yields the elastic modulus and indentation derived hardness. Note that the Oliver-Pharr method is based upon analysis of rate-independent elastic-plastic contact; however, it is of particular interest to investigate the behavior of rate-dependent plastic deformation of materials such as creep behavior.

Instrumented indentation creep tests are most often performed with load-time histories that utilize either a constant load-hold method, constant rate of loading, or constant strain rate [2]. In 1977, Chu *et al.* developed the impression creep method, which involves pressing a flat-end cylinder onto the test material under constant load and observing the depth increase [14-15]. The implementation of the flat-end indenter allows for a steady state penetration velocity at constant load. Results from this method have shown the indentation derived creep stress exponent ( $n$ ) and/or activation energy ( $Q$ ) are consistent with those measured by conventional uniaxial creep tests [14-15]. In regards to the commonly used sharp indenter geometries such as conical and pyramidal, the most practiced technique is the constant load-hold method, where the indentation is held at a fixed load over a duration of time while the indenter depth is monitored

[2,4,7,16-18]. The constant load-hold technique was first introduced by Pollock *et al.* and later refined during the research of Mayo *et al.*; where the indentation derived hardness, elastic modulus, and strain rate sensitivity for nanophase and single crystal TiO<sub>2</sub> were investigated [17]. It was discovered that with indentation depth increase, the hardness along with the indentation strain rate decreased with time [3].

The indentation strain rate is defined as the instantaneous descent rate of the indenter divided by that depth [14]

$$\dot{\epsilon}_i = \frac{1}{h} \left( \frac{dh}{dt} \right) \quad (7)$$

where  $h$  is the instantaneous indentation displacement and  $t$  is time. By monitoring the change in hardness and indentation strain rate during the indentation process, the stress exponent ( $n$ ) can be determined by means of Equation 2. Reasonable agreement with those measured by conventional uniaxial creep tests has been reported [16-19]; however, uncertainty errors exist from not achieving steady-state as hardness is time-dependent during the constant-load method [20].

The constant strain-rate method is less frequently used due to its comparatively difficult implementation; however, it holds significant practical interest. In attempt to eliminate the uncertainties encountered in the constant-load method, it was proposed that by holding the indentation strain-rate constant, steady-state may more easily be achieved [2, 8]. Oliver and Lucas [8] showed for the first time that the indentation strain rate could be held constant during an experiment by ensuring the loading rate divided

by the load,  $\frac{1}{P} \left( \frac{dP}{dt} \right)$ , to be constant. Oliver and Lucas used this method to investigate the creep response of high purity Indium. It was discovered that the yielded results exhibited good agreement with literature data for both the stress exponent (n) and the activation energy (Q). Further studies employing the constant strain-rate method have been reported [21, 22].

Numerous studies, independent of method, have shown satisfactory correlation of stress exponents (n) obtained through indentation and conventional uniaxial creep tests; however, there is very little experimental data in the literature investigating the correlation between the creep coefficients (A) [8,17,19]. Goodall and Clyne [20] discovered that the data measured from instrumented indentation tests did not correlate well with those reported in the literature obtained by conventional uniaxial tests. It was found that large discrepancies exist between the two creep rates; specifically, the indentation creep rate ( $\dot{\epsilon}_i$ ) is faster than the uniaxial creep rate ( $\dot{\epsilon}_s$ ). Poisl et al. [23] made efforts to correlate the indentation strain rate with the effective strain rate experienced by the material Selenium under the indenter. The ratio  $\frac{\dot{\epsilon}_s}{\dot{\epsilon}_i}$  was found to be approximately 0.09. Takagi et al. [16] also studied the relationship between  $\dot{\epsilon}_i$  and  $\dot{\epsilon}_s$  by examining the AL-Mg solid solution alloy with a stress exponent of three and obtained the ratio  $\frac{\dot{\epsilon}_s}{\dot{\epsilon}_i}$  of 0.28. It is still unclear whether or not these ratios are representative of other materials showing the power-law creep behavior; thus, research attempting to correlate the indentation and uniaxial strain rates holds high value.

## 1.4– Thesis Objective

Nano & micro advances with materials require mechanical characterization unattainable through traditional creep measurement methods intended for large bulk materials. Precise knowledge of these mechanical properties is essential in device specific functions and understanding its applications. Although instrumented indentation tests hold promise to numerous advantages, assessing creep behavior through instrumented indentation is not as straightforward to analyze and interpret as the more conventional uniaxial creep test [7], as was discussed above.

This study aims to gain insight on the relationship between indentation and uniaxial power-law creep. More specifically, it attempts to correlate the indentation strain rate,  $\dot{\epsilon}_i$ , and uniaxial strain rate,  $\dot{\epsilon}_s$ , from a numerical modeling standpoint. In doing so we will illustrate numerically that the indentation creep test will yield approximately the same stress exponent as in the uniaxial creep test. The power-law creep coefficient,  $A$ , will also be investigated through the strain rate ratio  $\frac{\dot{\epsilon}_s}{\dot{\epsilon}_i}$ .

An investigation comparing the indentation derived creep response through the constant load-hold and constant strain rate methods is to be performed. Attention is first devoted to tin (Sn)-based materials, which exhibit power-law creep behavior even at room temperature. The  $\dot{\epsilon}_i - \sigma$  relation for the Sn based materials will be compared with their uniaxial counterparts and the difference may be quantified. Secondly, in attempt to further understand the constant strain-rate method, a parametric analysis altering the stress exponent and creep constant will be performed.

The strain rate ratio  $\frac{\dot{\epsilon}_S}{\dot{\epsilon}_I}$  will be monitored as the power-law creep parameters vary. This analysis will give insight to parameter sensitivity and establish an accuracy domain. The numerical finding will thus provide quantitative guidance regarding the extraction of the power-law creep parameters via instrumented indentation.

## **Chapter 2: Model Description**

## 2.1 – Material Model

As mentioned in Chapter 1, attention is devoted to Sn-based materials due to their ability to display the power-law creep behavior even at room temperature. In particular, four material models are to be considered first: pure Sn at 25 °C, pure Sn at 120 °C, Sn-3.9Ag-0.7Cu alloy at 25 °C, and Sn-3.9Ag-0.7Cu alloy at 120 °C, all in their bulk form. *Sidhu et al.* [24] investigated the creep behavior of the four considered material models and have published the experimentally measured uniaxial steady-state power-law creep responses. Re-created from the linear fit in Ref [24], Figure 3 illustrates the experimental creep response of the four considered materials. The stress exponent ( $n$ ) may be extracted from the published strain-rate versus stress ( $\dot{\epsilon}_i$ - $\sigma$ ) curves, and is defined as the average slope along the  $\dot{\epsilon}_i$ - $\sigma$  curve. The simplified steady-state power-law creep relation at constant temperature (Equation 2) may be used to derive the creep constant ( $A$ ). The material model inputs used in the modeling are listed in Table 1 where the elastic and power-law creep parameters are defined. Note that temperature is not explicitly defined in the numerical model; however, its effect is considered through the input creep parameters.

Material Model	E [GPA]	$\nu$	A [ $s^{-1}MPa^{-n}$ ]	$n$
Sn at 25 °C	46	0.34	$1.24 \times 10^{-12}$	7
Sn at 120 °C	35	0.34	$2.20 \times 10^{-9}$	7
SnAgCu at 25 °C	46	0.34	$1.95 \times 10^{-22}$	10
SnAgCu at 120 °C	35	0.34	$2.0 \times 10^{-17}$	8

Table 1: Material Properties used in the constant load- hold and constant strain-rate model

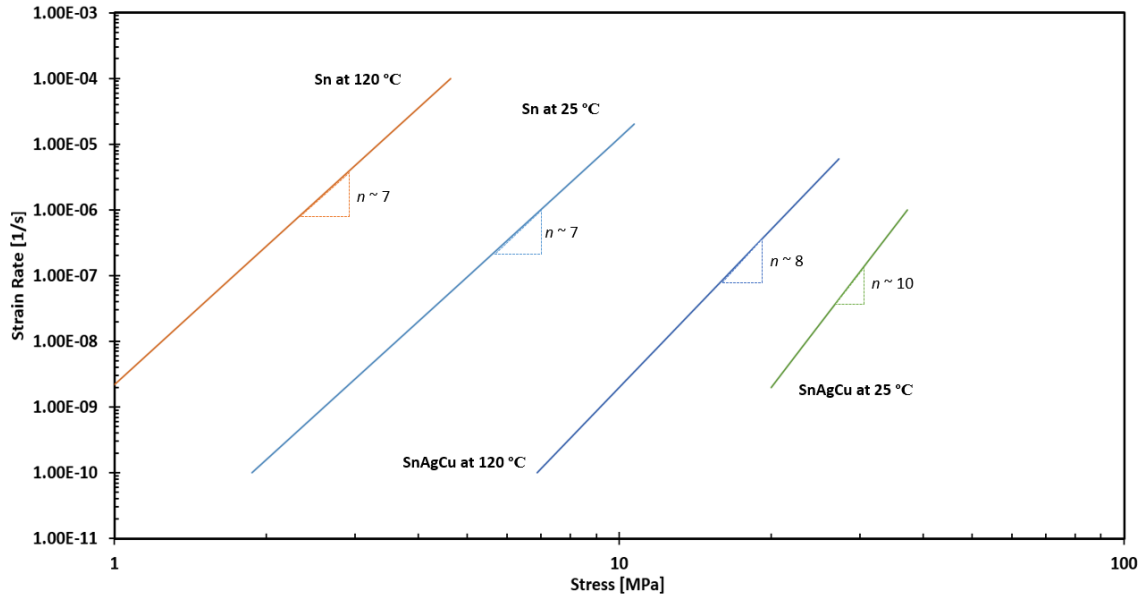


Figure 3: Experimentally measured steady-state creep response for the four material models considered, per Ref. [24]

The first half of this study is devoted to analyzing the creep response under the constant load-hold method; accordingly, the four material models described above will be assessed. The results yielded from the numerical model will be used to assess how this indentation creep technique can be used to extract uniaxial power-law creep data [24]. The second half of this study seeks to investigate the constant strain-rate method. The yielded results will be compared to the constant load-hold creep response. In addition to the four Sn based material models, an expanded parametric analysis is conducted, which seeks to further investigate the constant strain-rate method with material models of varying power-law creep parameters ( $A$  &  $n$ ).



## 2.2 – Constant Load-Hold Model

The numerical assessment is to be carried out using the finite element package ABAQUS (Version 6.12, Dassault Systems Simulia Corp., Providence, RI) [25]. The model geometry for the constant load-hold method is depicted in Figure 4, which shows a schematic of the indenter and test material, along with the boundary conditions and local mesh.

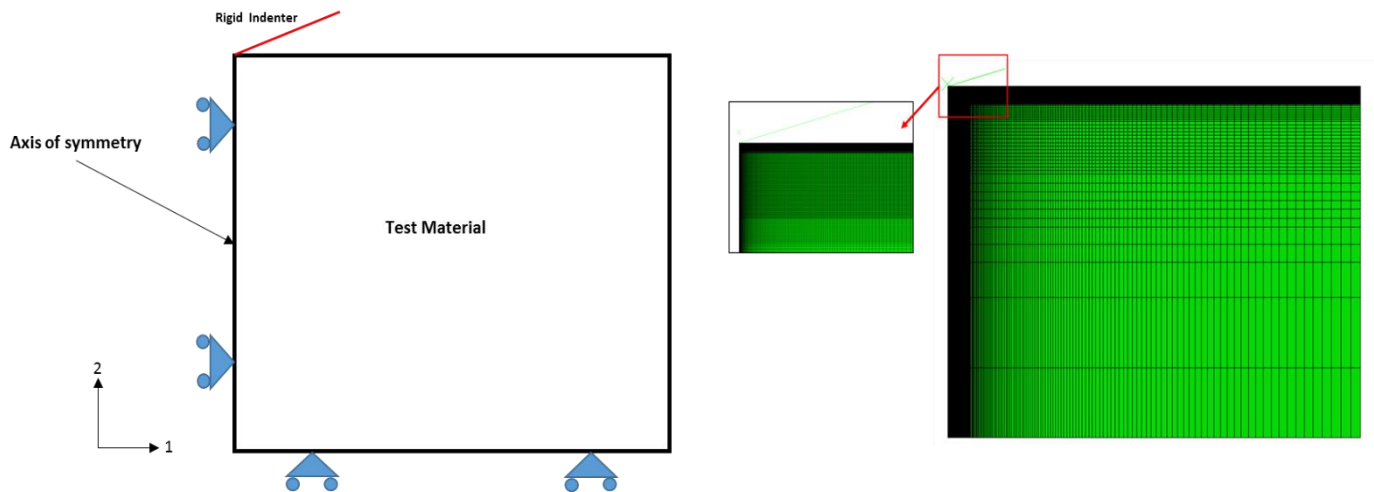


Figure 4: 2-D axisymmetric model schematic. LEFT: Constant load-hold model schematic. RIGHT: Model mesh for load-hold method

As previously mentioned, the model configuration consists of a test material and an indenter. The test material is modeled as a cylindrical homogeneous material with a lateral span (radius) of  $200\ \mu\text{m}$  and a height of  $200\ \mu\text{m}$ . The indenter is modeled as a rigid conical indenter with a semi-angle of  $70.3$  degrees. Use of a conical indenter is a practical way to model this type of indentation loading in a two-dimensional setting.

The test material is modeled as a two-dimensional axisymmetric problem utilizing four-node quadrilateral elements (CAX4). Note that CAX elements can be subjected to axially symmetric loading conditions; however, they do not support torsion loading [25]. The indenter is modeled as a perfectly rigid virtual line for simplicity, which is a standard assumption made in most indentation models [26-27]. Accordingly, the elastic modulus and Poisson's ratio of the indenter are  $E_i = \infty$  and  $\nu_i = 0$ , respectively. It is worth mentioning that with the assumption of a rigid indenter the second term in Equation 5 goes to zero if one intends to examine the indentation derived elastic behavior. As shown in Figure 4, a fine mesh is used in the vicinity of the contact region to capture localized deformation and stress gradients due to the indentation process. The mesh is also gradually coarsened away from the contact region to drive down computational costs. A more detailed description of the model mesh is provided in Section 2.4.

In accordance with the axisymmetric model, the nodes along the axis of rotation were constrained in the 1-direction and the corresponding nodes along the bottom surface of the test material were constrained in the 2-direction, see Figure 4. Lastly, the defined node representing the rigid indenter was constrained in the 1-direction and constrained from rotation about the 3-axis (in-plane). A prescribed coefficient of friction between the rigid conical indenter and the top surface was defined to be 0.1, which is a typical value for a diamond/metal contact pair [9-10].

In order to satisfy the constant load-hold method a total of three load steps were created and are tabulated in Table 2. During Step-1, a concentrated force was

applied to the reference node defining the rigid indenter. At 10 seconds the prescribed load is achieved and Step-2 is initiated. The concentrated force is then held for 30 hours and the time-dependent deformation (creep) is monitored. Step-3 commences once the hold period is complete and retracts the indenter to its original position. Each of the four Sn-based material models were subjected to two different peak forces, 50 $\mu$ N and 100 $\mu$ N.

Load Step	Procedure	Time
Step-1	Load	10 seconds
Step-2	Hold	30 hours
Step-3	Unload	10 seconds

*Table 2: Constant load-hold method – Load step conditions applied to the model*

In this method, the depth versus time (h-t) curve and the deformed configuration, during the holding period, will be used to extract the instantaneous contact radius as well as the depth rate; hence, enabling power-law creep response (namely strain rate – stress relationship) to be acquired.

### **2.3 – Constant Indentation Strain-Rate Model**

The above section focused primarily on the constant load-hold method; however, the constant indentation strain-rate method is an alternative indentation creep technique and should thus be examined. The model geometry for the constant indentation strain-rate method is depicted in Figure 5, which shows a schematic of the indenter and test material, along with the boundary conditions and local mesh.

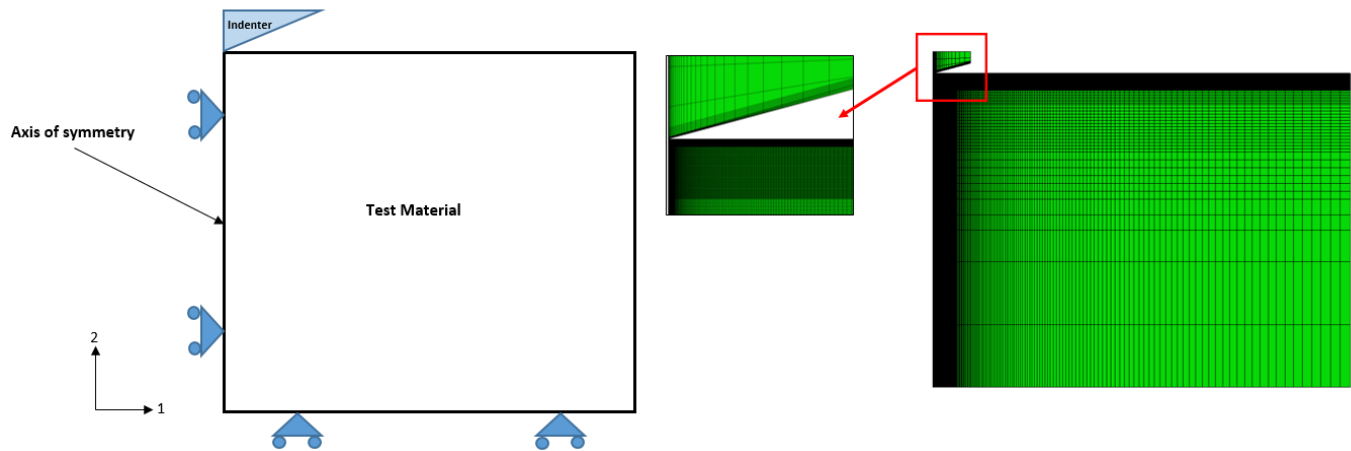


Figure 5: 2-D axisymmetric model schematic. LEFT: Constant strain-rate model schematic. RIGHT: Model mesh for constant strain-rate method

By visual inspection of Figures 4 & 5, it is observed that the test configuration for the constant strain-rate method is essentially the same as the constant load-hold method. Despite their similarities the constant strain-rate model holds two distinct differences; the implementation of a non-rigid diamond indenter and the prescribed loading conditions.

The implementation of a conical diamond indenter allows the indenter to respond elastically while being driven in and out of the material surface. The Young's modulus and Poisson's ratio of the elastic diamond indenter are 1,141 [GPa] and 0.07, respectively [3]. It may be justified that the diamond indenter is in contact with a compliant material considering the diamond indenter is significantly stiffer than the Sn-based material. According to Fischer-Cripps [28], even if the deformation of the indenter

is accounted for the result is essentially equivalent to a rigid indenter in contact with a compliant material. Therefore, the reason for modeling the non-rigid diamond indenter in this part of the thesis was to ensure model consistency, for result comparison, between the constant strain-rate models developed in [13].

During indentation, displacement ( $h$ ) is applied to all nodes attached to the top surface of the indenter. The rate of loading is such that indentation strain-rate ( $\dot{\epsilon}_i$ ), defined in Equation 2, maintains a set constant. This is achieved in a piecewise manner, through successive intervals with an increasing displacement rate up to a maximum indentation depth of  $4\mu\text{m}$  [13]. This study considers indentation strain-rates,  $\dot{\epsilon}_i$ , ranging from  $10^{-7}$  to  $10^{-4} [\text{s}^{-1}]$ . For example, consider the constant strain-rate to be  $\dot{\epsilon}_i = 10^{-4} [\text{s}^{-1}]$  and the maximum indentation depth of  $4\mu\text{m}$  with 10 piecewise load steps. The corresponding model inputs for each load step are shown in Table 3. The calculated time at each depth ensures that a constant strain rate of  $10^{-4} [\text{s}^{-1}]$  is achieved.

Strain Rate =0.0001 [1/s]			
STEP	h [um]	h_dot [um/s]	time [s]
1	0.4	0.00004	10000
2	0.8	0.00008	5000
3	1.2	0.00012	3333.333
4	1.6	0.00016	2500
5	2	0.0002	2000
6	2.4	0.00024	1666.667
7	2.8	0.00028	1428.571
8	3.2	0.00032	1250
9	3.6	0.00036	1111.111
10	4	0.0004	1000

Table 3: Constant indentation strain-rate method – Model inputs for each load step ensuring constant  $\dot{\epsilon}_i$

In this method, post-processing occurs at the onset of unloading, the end of load Step-10; accordingly, the maximum reaction force and maximum contact radius may be

extracted. These parameters enable the hardness and creep stress at a specific strain-rate to be derived. Table 3 only displays the model inputs for a constant strain-rate of  $10^{-4} [s^{-1}]$ ; accordingly, three more constant strain-rate simulations need to be completed in order to obtain a complete  $\dot{\epsilon}_i$ - $\sigma$  creep response.

One of the objectives of this thesis research is to compare the constant load-hold method and constant indentation strain rate method, using systematic numerical modeling. There appears to be no experimental work in the open literature comparing the two methods applied to the same material. In Ref. [29], sufficient experimental information is provided which enables a preliminary comparison. The data therein are analyzed in Appendix A of this thesis, as a partial validation of the methodology considered in the present numerical study.

## 2.4 – Mesh Convergence

In finite element modeling, a finer mesh typically results in a more accurate solution. However, as a mesh is made finer, the computation time increases. A mesh convergence study is performed in order to determine a mesh that satisfactorily balances accuracy and computing resources. Three mesh schemes were developed and mesh convergence was checked through the modeled indentation hardness values at different indenter depths. Table 4 displays the database summary for each mesh density model.

<b>Mesh</b>	<b>1</b>	<b>2</b>	<b>3</b>
Elements	928	61,608	75,897

*Table 4: Database summary of each mesh*

Per Figure 6, Mesh-1 model consists of 928 elements and is refined in the upper left region to capture the localized deformation caused by the indenter. The mesh is also gradually coarsened away from the contact region. Indentation is an extremely severe form of deformation with very high local strains and sharp gradients. As observed in Figure 9, the minimal amount of elements in Mesh-1 is limiting the model from generating consistently accurate results; however, the obtained hardness value agrees with the overall trend of the other two meshes. Mesh-2 was developed in a similar manner as Mesh-1; however, a significant refinement was applied to this mesh model, see Figure 7. The total amount of elements increased to 61,608. Mesh-3 was developed using a different methodology approach. A uniform zone, 25 x 25 [ $\mu\text{m}$ ], located at the upper left corner was defined, see Figure 8. A uniform mapped mesh refinement was then applied to the indentation zone yielding a total of 75,897 model elements. Beyond the indentation zone there is no need for a fine mesh scheme; accordingly, the mesh transitions from fine to coarse as we move away from the indentation zone.

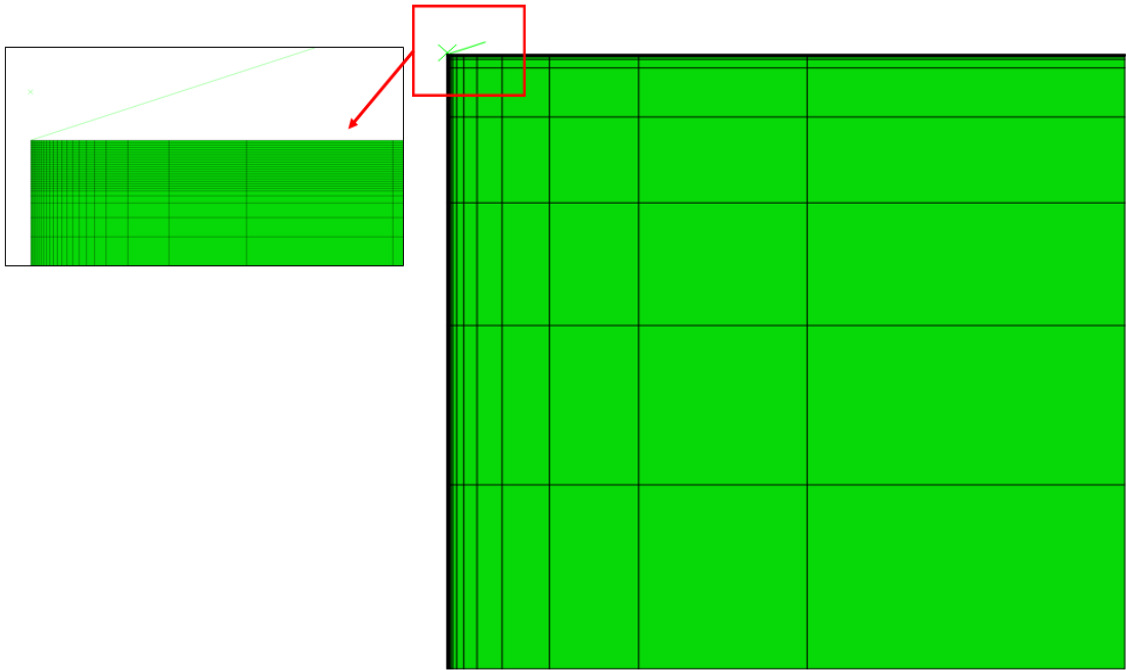


Figure 6: Mesh 1

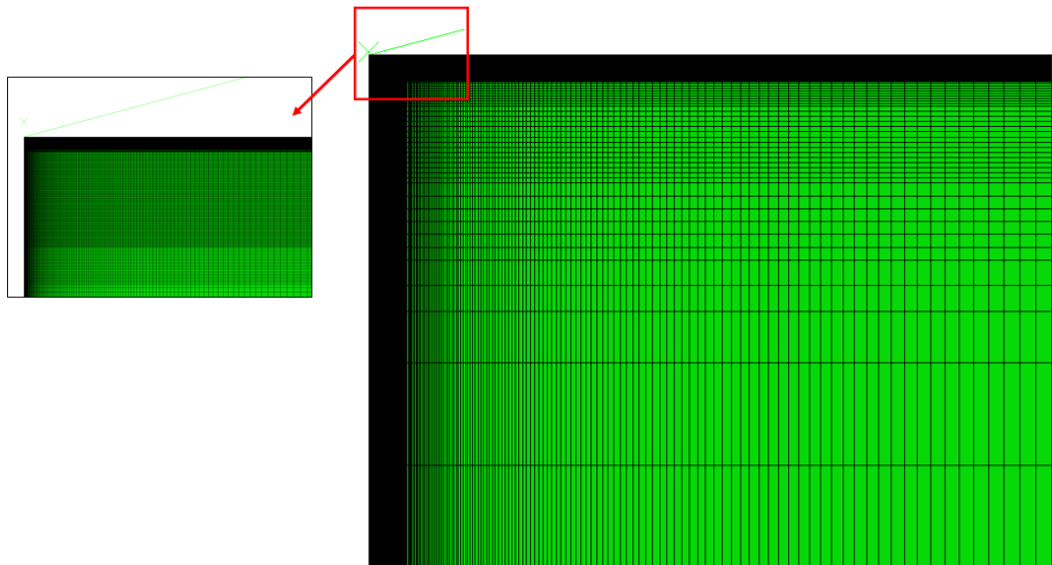


Figure 7: Mesh 2



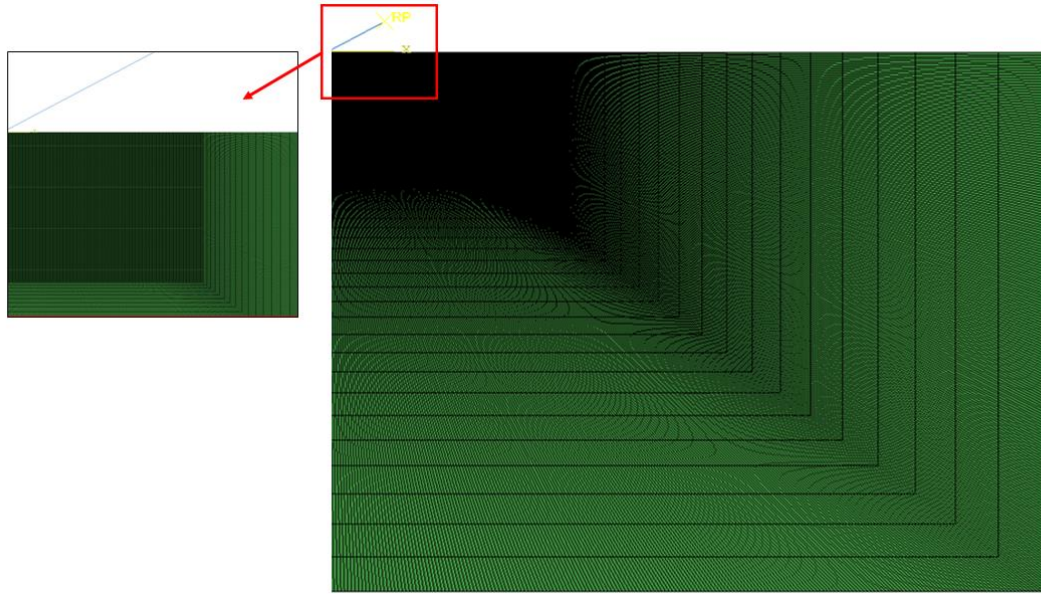


Figure 8: Mesh 3

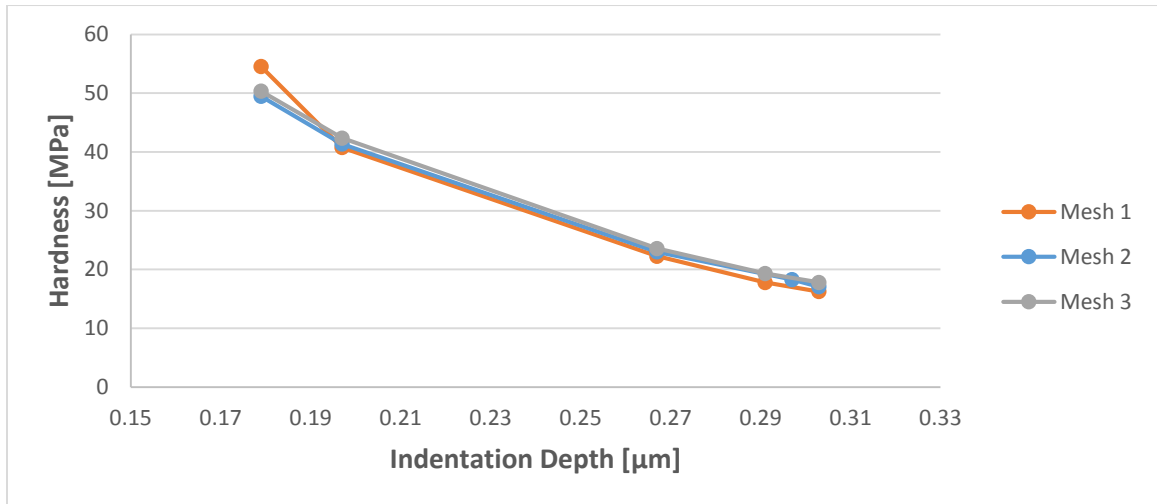


Figure 9: Convergence study

It can be seen in Figure 9 that the results from these three mesh models are in reasonable agreement and the hardness values are within 2% from each other, with the exception of the Mesh-1 outlier. As previously mentioned, the minimal amount of elements in Mesh-1 limit the model from generating consistently accurate results. The

hardness is consistently lower than the other two mesh models except at a depth of about 0.18 $\mu\text{m}$ . Here the hardness value is larger than those of the refined mesh models. Mesh-3 showed promising hardness results when comparing to Mesh-2; however, the computational cost was significant. Mesh 2 model was chosen as the optimal model to complete the rest of the analysis for this study. This model was the most time efficient and the results were not compromised due to the reduced amount of elements.

## **Chapter 3: Constant Load-Hold Method**

### 3.1 – Constant Load-Hold Method

The first objective of this study is to investigate the indentation derived creep response through a constant load-hold method. As described in Section 2.2, two separate runs will be performed for each of the four Sn-based material models, one with a peak load of 50 $\mu$ N and the other 100 $\mu$ N. Again, the three load steps defining this model are tabulated in Table 2 and can be visually represented in Figure 10. In this method, several points along the depth-time ( $h-t$ ) curve during the hold period are picked and processed in order to determine the correlation between indentation derived strain rate ( $\dot{\epsilon}_i$ ) and creep stress ( $\sigma$ ). The creep stress is taken as [13, 16, 23]:

$$\sigma = \frac{H}{3} \quad (8)$$

where  $H$  is hardness as defined in Equation 6. The  $\dot{\epsilon}_i - \sigma$  relation for the four Sn-based materials may then be compared with their uniaxial counterparts ( $\dot{\epsilon}_s - \sigma$  relation), and the difference can be quantified.

To further demonstrate this process, consider pure Sn at 120 °C. Figure 10 displays the simulated load-depth response of pure Sn at 120 °C under peak loads of 50  $\mu$ N and 100  $\mu$ N. It is observed during the constant hold stage that a significantly larger depth penetration is achieved at the higher peak load. In other words, the higher the peak load, the more significant the creep effect. It is also worth mentioning that the overall depth achieved for the smaller peak load of 50  $\mu$ N is 34% smaller than the higher peak load of 100  $\mu$ N. This observation holds true for all of the Sn-based material models analyzed in this section of the study.

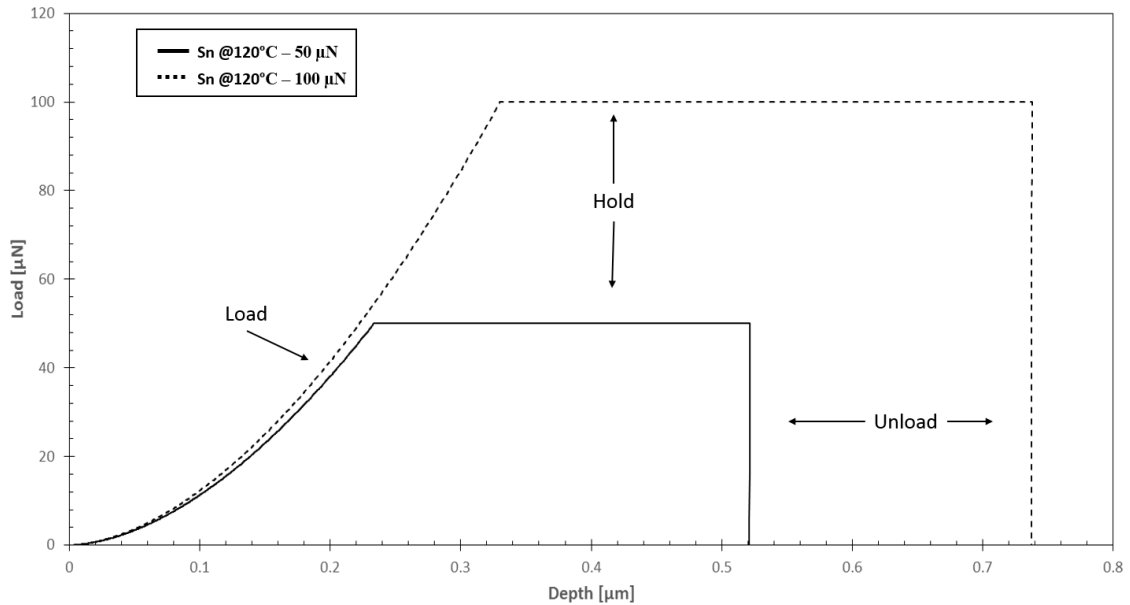
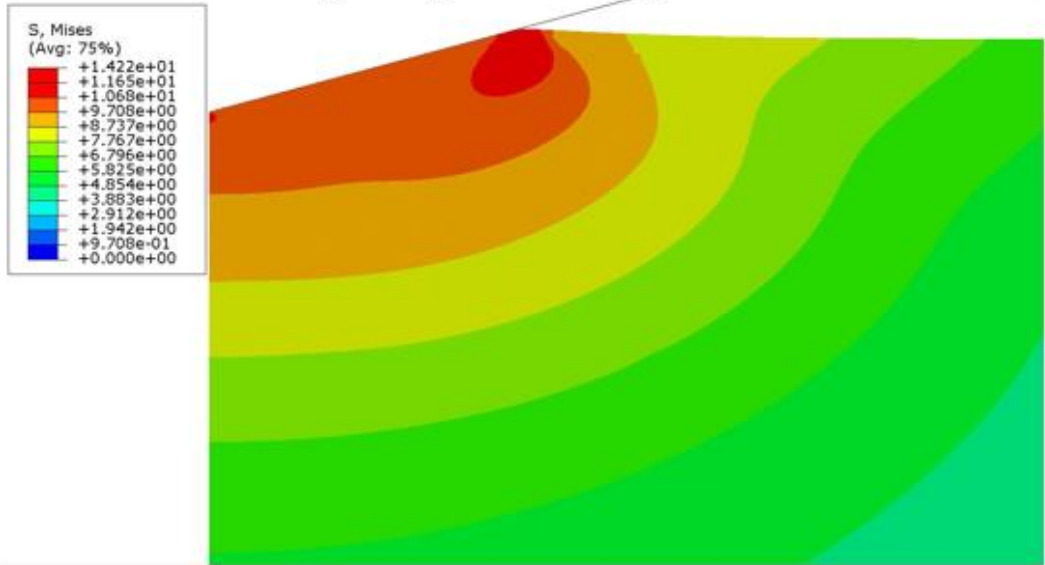


Figure 10: Simulated (P-h) Load-Depth response of pure Sn at 120°C under two different peak loads

Representative contour plots in the deformed configuration are presented in Figures 11-14. Again, pure Sn at 120 °C is the investigated material model. Figures 11 (a) and (b) show the contour plots of Von Mises effective stress where the applied peak load is 50  $\mu\text{N}$  and indentation is at the beginning and end of the holding stage (30 hours), respectively. It is observed during the constant hold period that significant stress relaxation occurs with the higher stress regions relaxing more; thus, yielding a relatively uniform stress field. It can be shown in Figure 12 that a similar trend occurs with a larger applied peak load of 100  $\mu\text{N}$ ; however, the Von Mises effective stress at the beginning of the holding stage is higher. This observation serves as a sanity check as intuition tells us that an increase in applied peak load results in an initial increase in Von Mises effective stress.

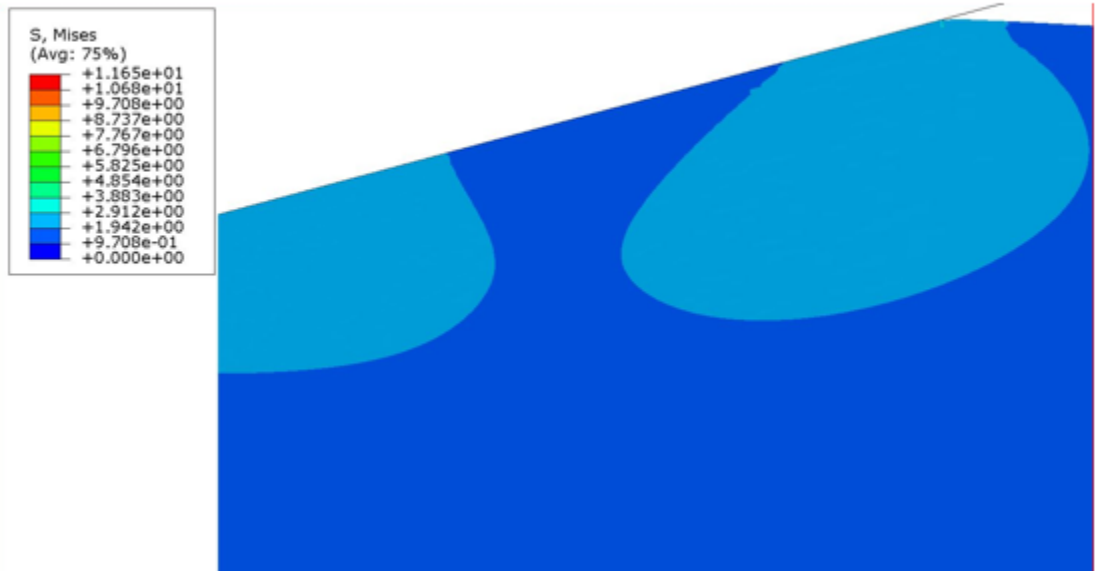
Figures 13 (a) and (b) show the contour plots of equivalent creep strain where the applied peak load is 50  $\mu\text{N}$  and indentation is at the beginning and end of the holding stage (30 hours), respectively. Upon initial inspection of Figure 13 the equivalent creep strain gradients for both peak load cases exhibit a similar trend. For this reason, the mesh framework is included in the equivalent creep strain contour plots to assist in the reasoning. It is observed that severe creep deformation occurs during the constant hold period as the affected area propagates throughout the duration of the holding period. It can also be shown in Figure 14 that pure Sn at 120 °C under a higher load displayed a similar trend of severe creep deformation during the constant hold period.

- Sn at 120°C
- Peak Load - 50μN
- Beginning of hold stage



(a)

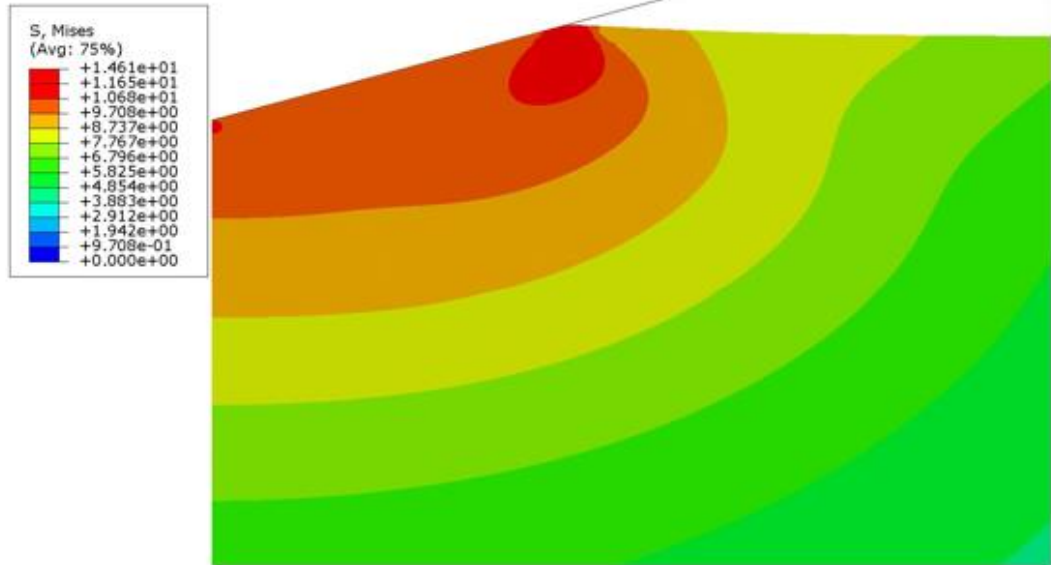
- Peak Load - 50μN
- End of hold stage (30 hrs)



(b)

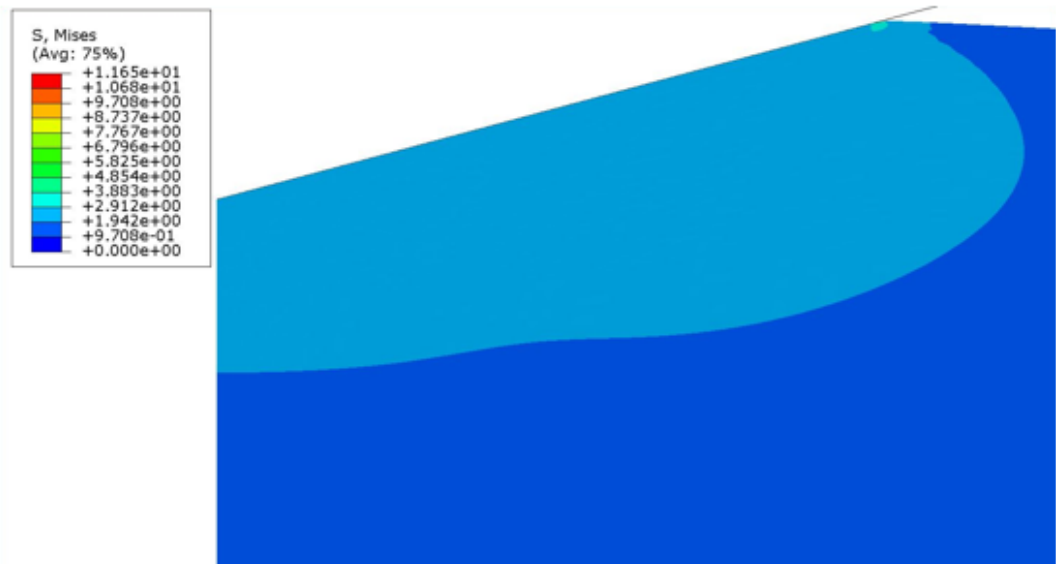
Figure 11: Contour plots of Von Mises stress for the model Sn at 120 °C, with a peak load of 50μN. Indentation is at (a) the beginning of the holding stage (b) the end of the holding stage (30 hours)

- Sn at 120°C
- Peak Load - 100μN
- Beginning of hold stage



(a)

- Peak Load - 100μN
- End of hold stage (30 hrs)

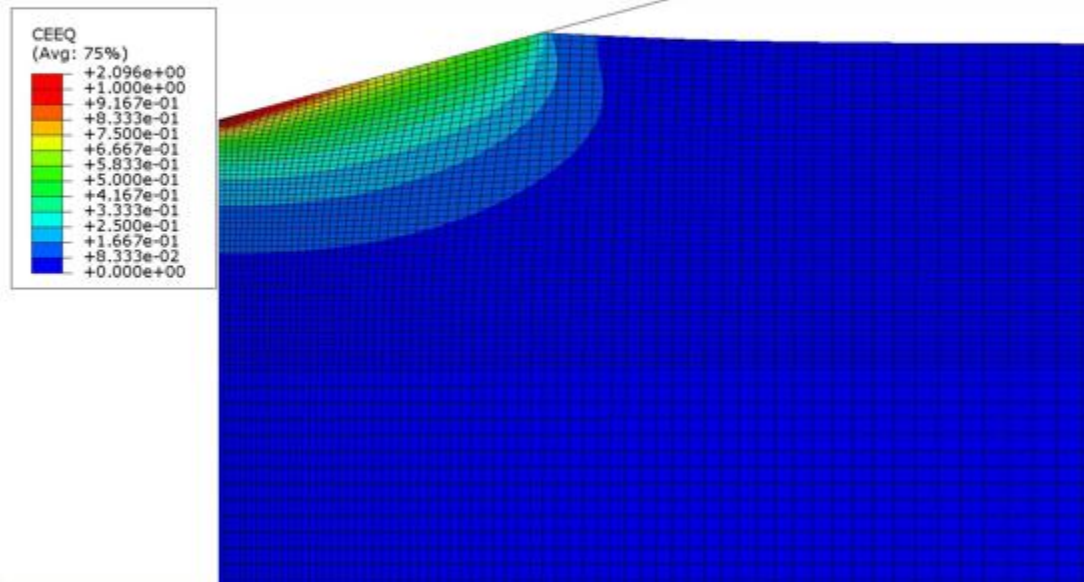


(b)

Figure 12: Contour plots of Von Mises stress for the model Sn at 120 °C, with a peak load of 100μN. Indentation is at (a) the beginning of the holding stage (b) the end of the holding stage (30 hours)

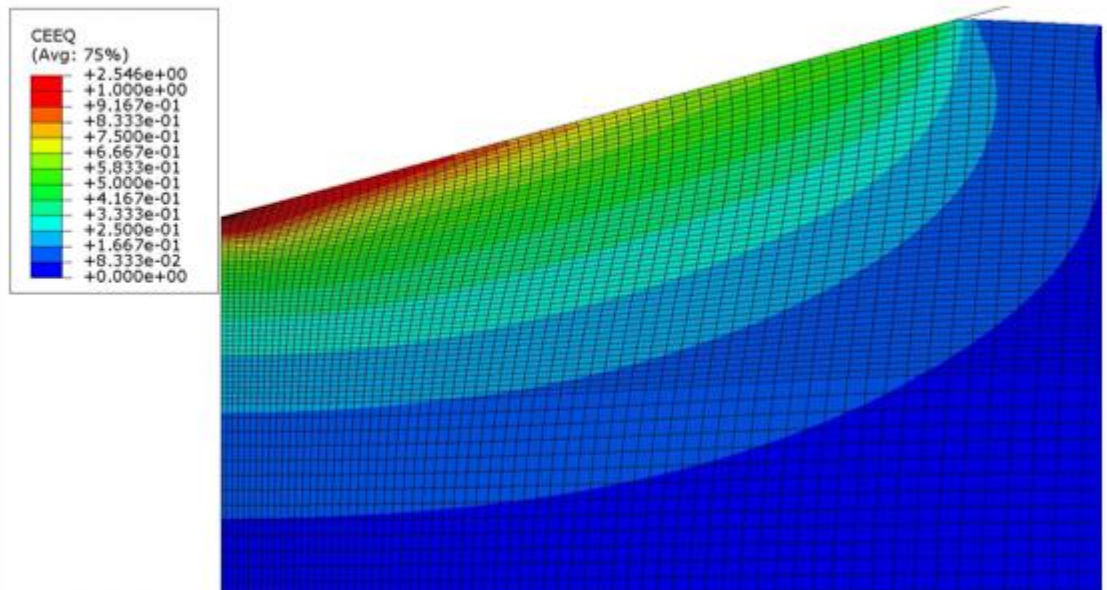


- Sn at 120°C
- Peak Load - 50μN
- Beginning of hold stage



(a)

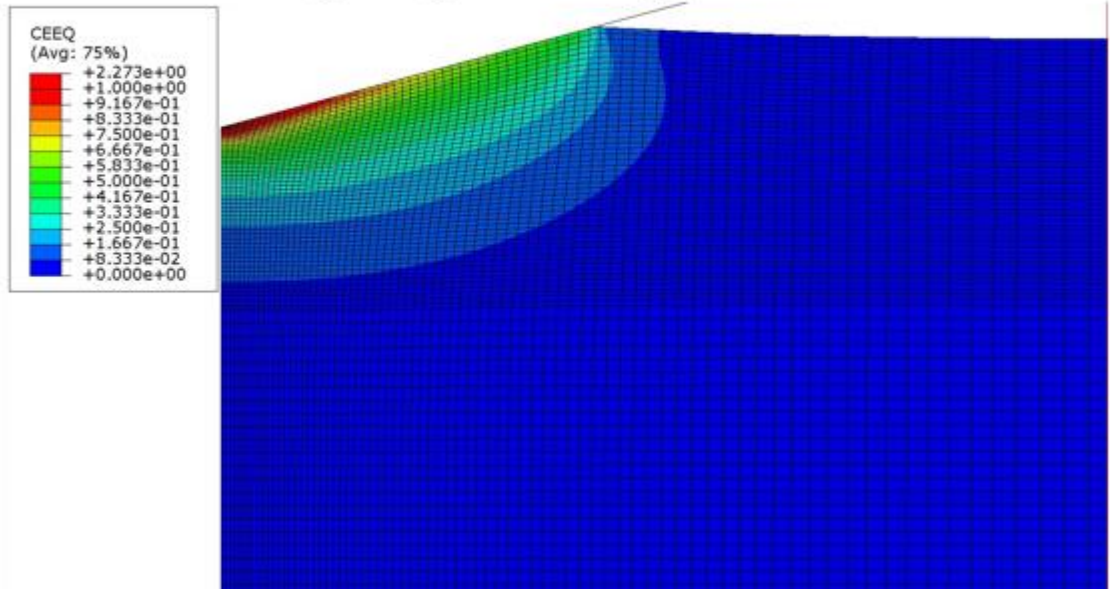
- Peak Load - 50μN
- End of hold stage (30 hrs)



(b)

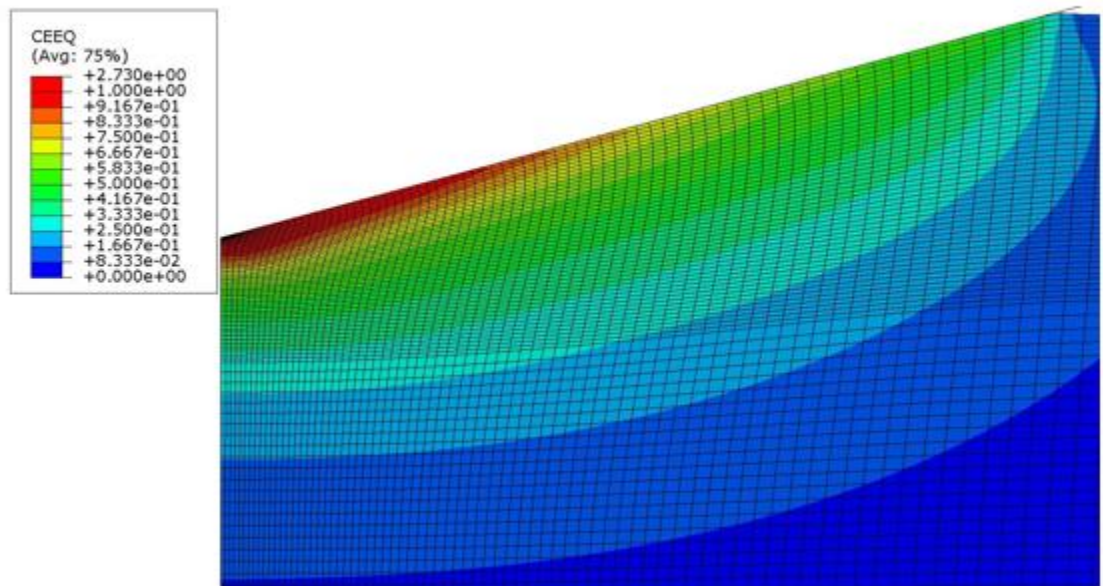
Figure 13: Contour plots of Equivalent Creep Strain for the model Sn at 120 °C, with a peak load of 50μN. Indentation is at (a) the beginning of the holding stage (b) the end of the holding stage (30 hours)

- Sn at 120°C
- Peak Load - 100μN
- Beginning of hold stage



(a)

- Peak Load - 100μN
- End of hold stage (30 hrs)



(b)

Figure 14: Contour plots of Equivalent Creep Strain for the model Sn at 120 °C, with a peak load of 100μN. Indentation is at (a) the beginning of the holding stage (b) the end of the holding stage (30 hours)

The constant load-hold method focuses exclusively on the creep behavior during the holding stage of indentation. From the data obtained during the holding stage, a depth-time curve ( $h-t$ ) may be constructed. Figure 15 represents the simulated  $h-t$  response for pure Sn at 120 °C. From the  $h-t$  data, the instantaneous contact radius ( $a$ ) and depth rate ( $\frac{dh}{dt}$ ) are calculated. This is achieved by picking several points (times) along the curve and for each time, observe the last nodal point in contact with the indenter [3]. The contact radius may then be determined by locating the 1-coordinate of the last node in contact at that specific time. The depth rate ( $\frac{dh}{dt}$ ) may be obtained by calculating the point slope of each selected point. Together with the depth rate ( $\frac{dh}{dt}$ ) and contact radius at each point, the indentation strain-rate and corresponding hardness can then be calculated. Finally, Equation 8 is utilized to establish an  $\dot{\epsilon}_i - \sigma$  relation.

The hold phase in the model allows outputs of depth and load results every increment; thus, generating a smooth continuous  $h-t$  curve. Taking this into consideration, there are countless combinations of points that may be chosen to carry out this analysis. To the best of our knowledge an accepted procedure regarding the point selection has yet been established. To avoid uncertainty regarding the choice of points along the  $h-t$  curve an experimental standard was created and applied to each material model. This standard required that both peak load simulations use the same time upon point selection with depth being the only varying parameter. For example, consider the  $h-t$  curve of pure Sn at 120° C, see Figure 15. Five points were distributed throughout the 30 hour holding period. As defined by the experimental standard both

the 50  $\mu\text{N}$  and 100  $\mu\text{N}$  load cases used the same time parameter during the point selection procedure. This procedure was repeated for each of the four Sn-based material models and each h-t response is depicted in Figure 16.

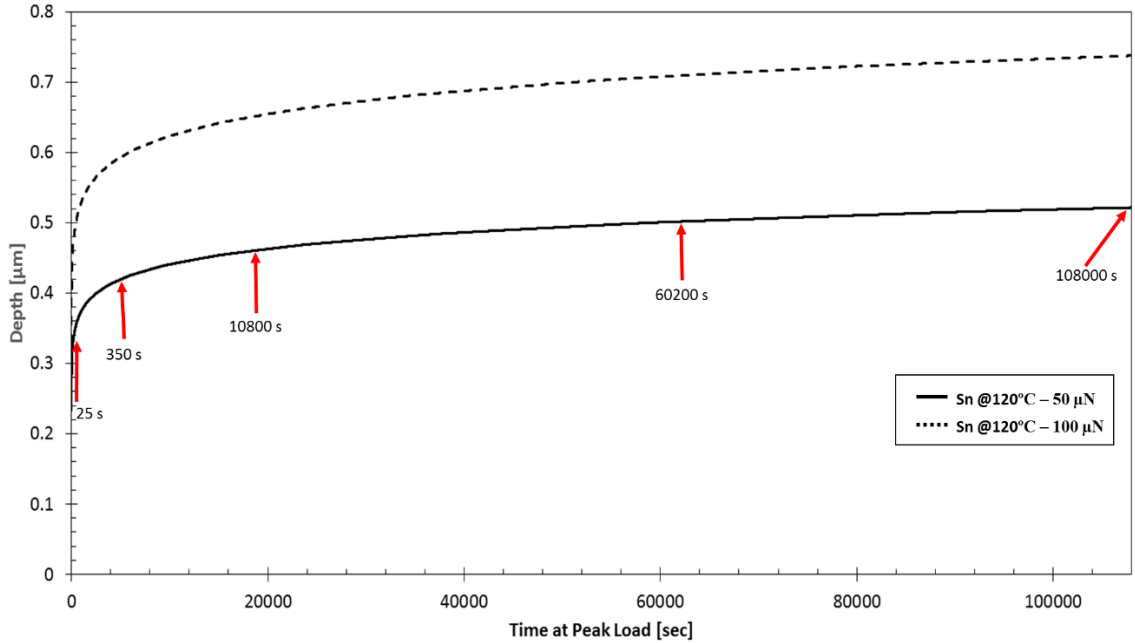


Figure 15: Simulated (h-t) Depth-Time response for pure Sn at 120°C under two different peak loads. Time duration of 30 hours.

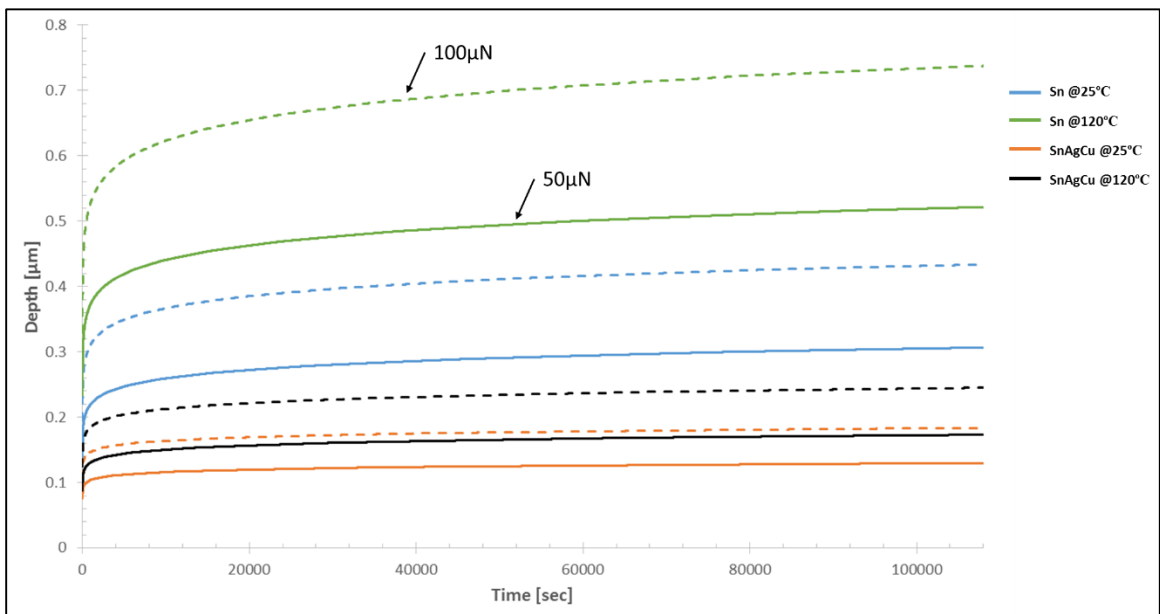


Figure 16: Simulated (h-t) Depth-Time response for the four Sn-based material models considered under two different peak loads

The simulated relationship between indentation strain rate and creep stress is plotted in Figure 17 (solid lines). The dashed lines represent the uniaxial power-law creep relations, based on Ref [24] and used as the model input. Note that the dashed power-law lines in Figure 17 are a direct representation with possible linear extension of the experimental results shown in Figure 3. This allows for easier comparison between indentation creep and conventional uniaxial creep over a consistent range of strain rates. The material models considered in this analysis yield an  $\dot{\epsilon}_i - \sigma$  relation with the strain rate and creep stress values spanning from  $1 \times 10^{-6}$  to  $1 \times 10^{-3} \text{ s}^{-1}$  and 1.9 to 65 MPa, respectively. It is observed that the two different peak loads result in very similar curves and are generally linear, so they are not easily discerned. It is also worth noting that upon initial observation of Figure 17, the indentation derived curves are nearly parallel to the uniaxial creep response of the respective material. The stress exponent ( $n$ ) is defined as the slope of the curve in the  $\dot{\epsilon}_i - \sigma$  relation on the log scale; accordingly, the indentation derived stress exponents are listed in Table 5. Note that the derived stress exponents of the two different peak loads are essentially equivalent, thus deeming the parameter independent of peak load. Comparing the  $n$  values in Table 1 & 5, it is confirmed that the stress exponent for a given material may be accurately obtained through the constant load-hold method. The satisfactory correlation of stress exponents ( $n$ ) is widely known; however, there is very little experimental data in the literature investigating the correlation between the creep coefficients ( $A$ ) [8,17,19].

The consistent parallel nature of the indentation and uniaxial creep behavior makes possible a meaningful determination of the quantitative difference between indentation strain rate and uniaxial strain rate [13]. In this work, the average vertical distance between the two curves was calculated and normalized as the ratio of indentation strain rate against uniaxial strain rate ( $\frac{\dot{\epsilon}_s}{\dot{\epsilon}_i}$ ). The calculated strain rate ratios ( $\frac{\dot{\epsilon}_s}{\dot{\epsilon}_i}$ ) are presented in Table 5. It was determined that for a specific material under different peak loads, the calculated ratio exhibited reasonable consistency with the largest discrepancy of 6% occurring in SnAgCu at 120 °C. When comparing the ratio of all four Sn-based material models, the value of  $\frac{\dot{\epsilon}_s}{\dot{\epsilon}_i}$  spans from 0.31 to 0.42 with the largest discrepancy of 30% occurring between pure Sn at 120 °C (the weakest material among the four) and SnAgCu at 25 °C (the strongest among the four). There is a tendency of increasing  $\frac{\dot{\epsilon}_s}{\dot{\epsilon}_i}$  as the creep resistance of the material increases.

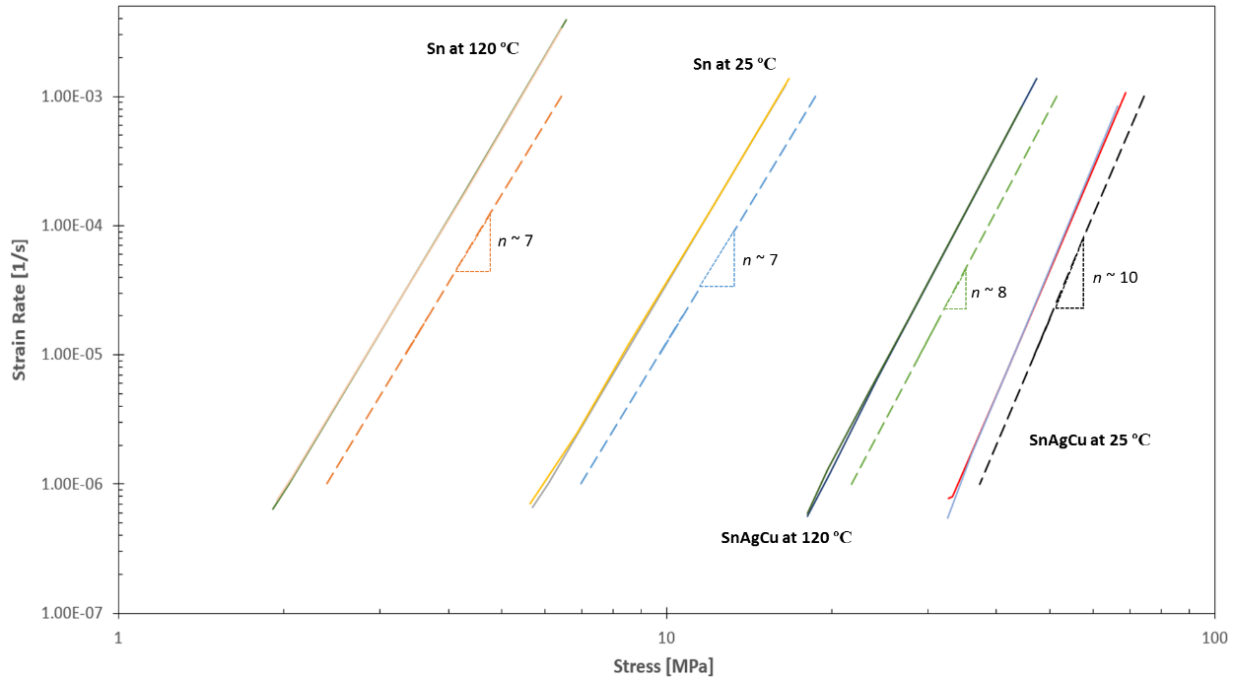


Figure 17: Relationship between indentation strain rate and creep stress, obtained from the indentation modeling (solid lines). The dashed lines represent the power-law creep relations, based on Ref [24] and used as the model input.

Material	Load [ $\mu\text{N}$ ]	$n$	$\dot{\epsilon}_s / \dot{\epsilon}_i$
Sn at 25 °C	50	7.081	0.351
	100	7.007	0.338
Sn at 120 °C	50	7.088	0.319
	100	7.037	0.316
SnAgCu at 25 °C	50	9.793	0.401
	100	10.196	0.425
SnAgCu at 120 °C	50	8.084	0.383
	100	7.999	0.36

Table 5: Stress exponent and strain-rate ratio obtained from constant load-hold model

**Chapter 4: Constant Indentation Strain Rate Method: Parametric  
Analysis**



## 4.1 – Constant Indentation Strain Rate Method

The second objective of this study is to investigate the indentation derived creep response through a constant indentation strain rate method. As described in Section 2.3, a constant strain rate may be attained by imposing a constant normalized load rate. Again, this is achieved in a piecewise manner through ten successive intervals with each interval increasing its displacement rate up to the maximum indentation depth of 4 $\mu$ m [13]. In this method, the maximum applied load ( $P_{max}$ ) and corresponding contact radius ( $a$ ) are extracted through ABAQUS Post-Processor [25] and used in Equations 6 & 8 to generate the  $\dot{\epsilon}_i - \sigma$  relation of the material. In this section, we will first investigate the four Sn-based material models under the imposed constant indentation strain rates ( $\dot{\epsilon}_i$ ) of  $10^{-7}$ ,  $10^{-6}$ ,  $10^{-5}$  and  $10^{-4}$  [ $s^{-1}$ ].

To gain a better understanding of creep behavior under the constant indentation strain rate method, consider the Sn-based alloy SnAgCu at 25 °C. Figure 18 shows the simulated load-depth response of SnAgCu at 25 °C under the four prescribed strain rates, ranging from  $10^{-4}$  [ $s^{-1}$ ] to  $10^{-7}$  [ $s^{-1}$ ]. It is observed that the rate effect is indeed significant, as a higher indentation strain rate results in a harder response. This observation is confirmed in Figure 19 where the simulated hardness ( $H$ ) is plotted as a function of indentation depth. Again, it is easily observed that hardness increases as the strain rate increases. It is also important to note that the hardness value stays relatively constant regardless of indentation depth. This observation illustrates that a steady state is established using the constant strain rate method – a feat that the constant load-hold

method was unable to accomplish due to continuous deviation from the steady state creep condition [20]. These observations hold true for the other three Sn-based material models; however, the load-displacement and hardness-depth curves are only shown for SnAgCu at 25 °C due to the repetitiveness of the results.

Representative contour plots in the deformed configuration are presented in Figures 20-21. Figures 20 (a) and (b) show the contour plots of equivalent creep strain for SnAgCu at 25 °C at a depth of 4 [μm] with a prescribed indentation strain rate of  $10^{-4}$  [ $s^{-1}$ ] and  $10^{-7}$  [ $s^{-1}$ ], respectively. It can be seen that both contour plots of equivalent creep strain are virtually indistinguishable regardless of the prescribed strain rate. This is expected as both cases are in the same deformation state at a depth of 4 [μm]. In order to gain better insight into the rate effect phenomena it is worthwhile to observe the Von Mises stress contour plots in Figure 21. Figures 21 (a) and (b) show the contour plots of Von Mises effective stress for SnAgCu at 25 °C at a depth of 4 [μm] with a prescribed indentation strain rate of  $10^{-4}$  [ $s^{-1}$ ] and  $10^{-7}$  [ $s^{-1}$ ], respectively. It is observed that as the strain rate increases; the material located directly beneath the indenter experiences larger stress concentrations. This agrees well with the observations made from Figures 18-19 where it was found that higher strain rates yield a harder material response.

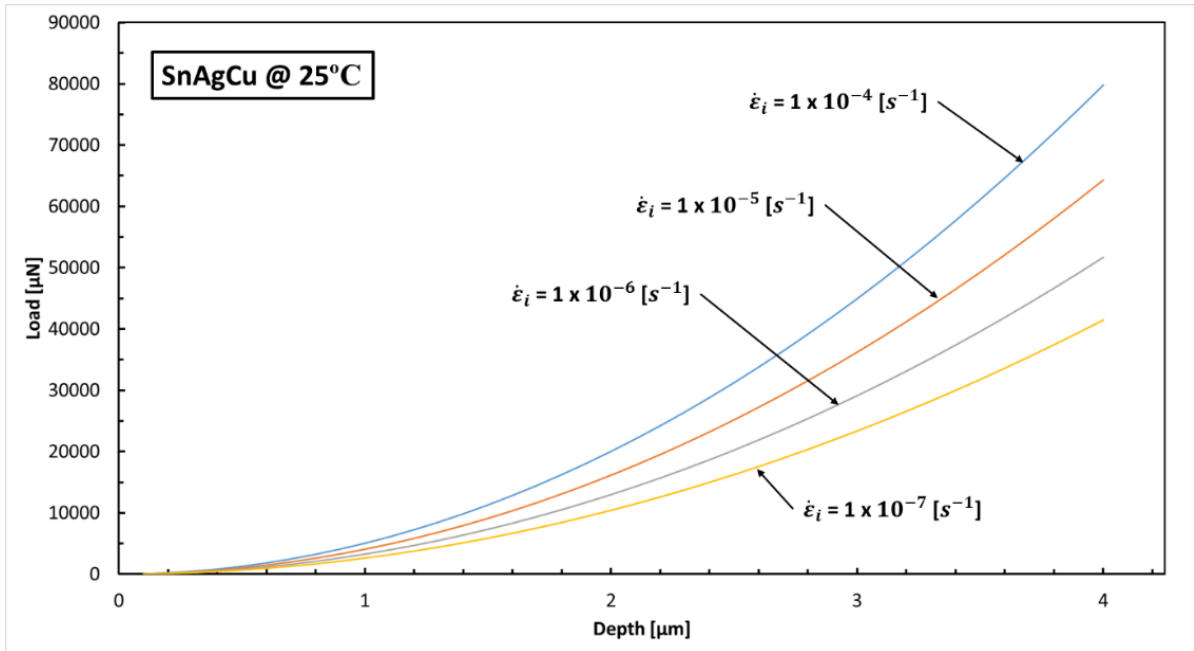


Figure 18: Simulated load-displacement response of SnAgCu at 25 °C under four different strain rates

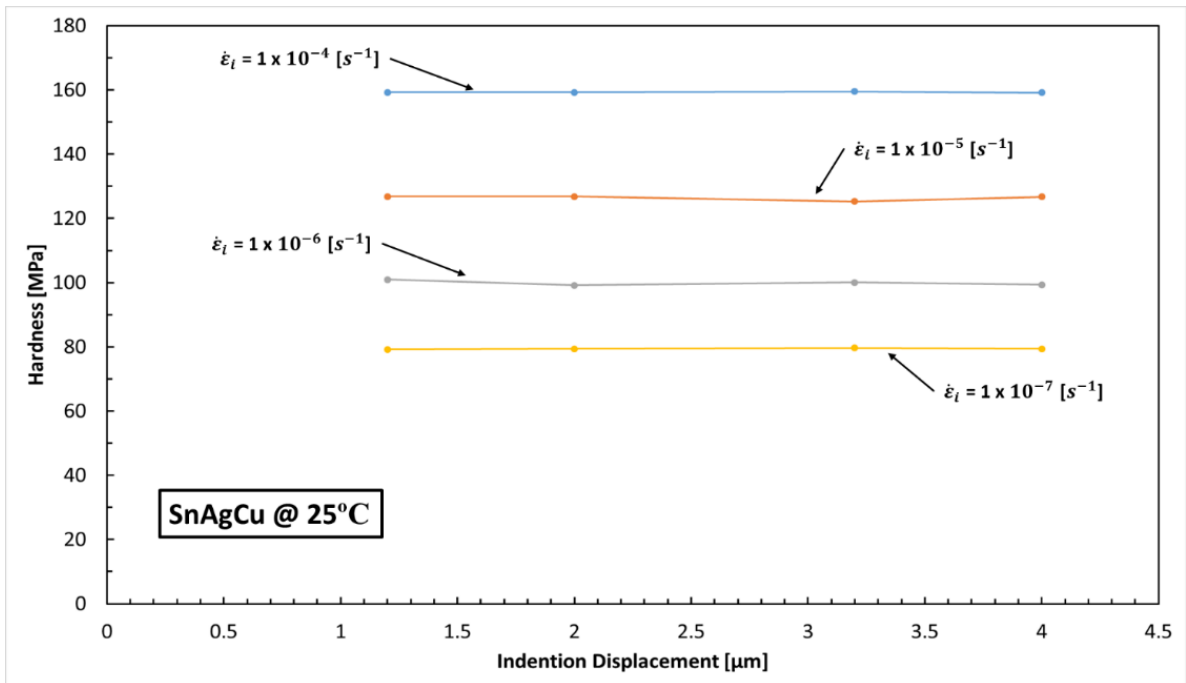
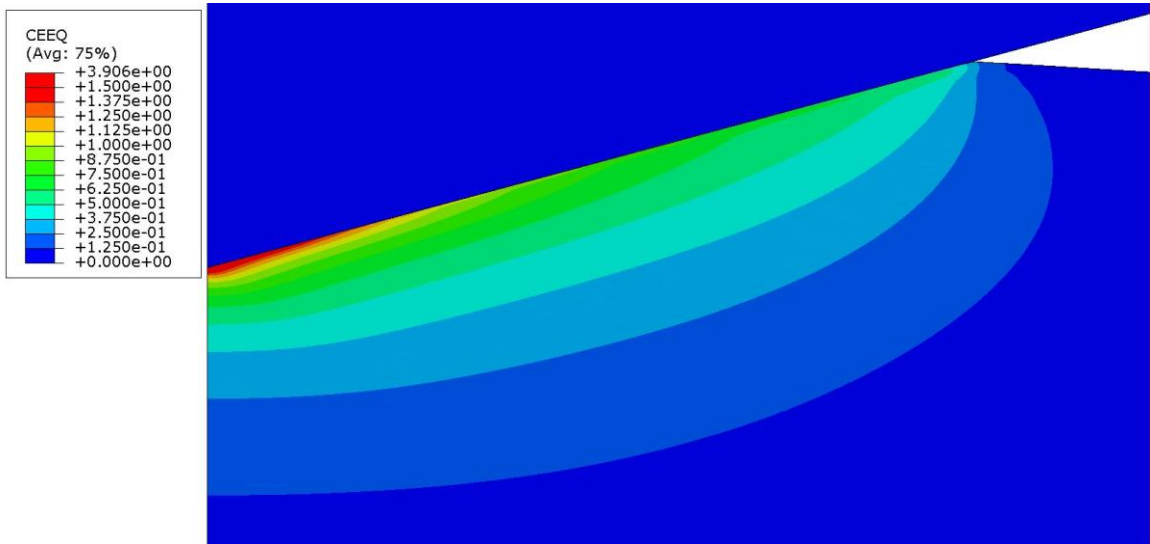
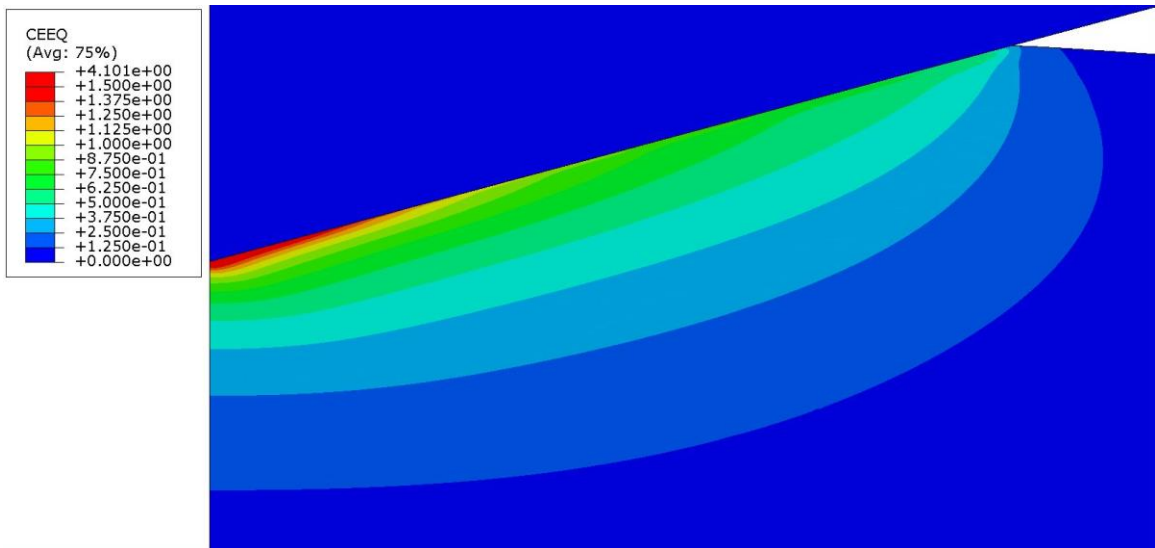


Figure 19: Simulated hardness as a function of indentation displacement for SnAgCu at 25 °C

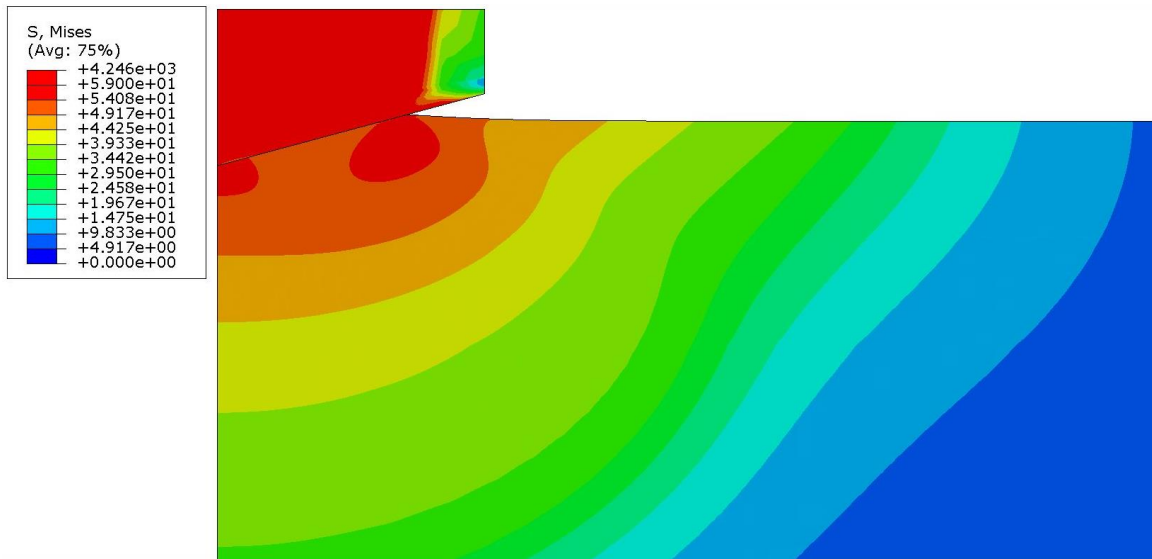


(a)

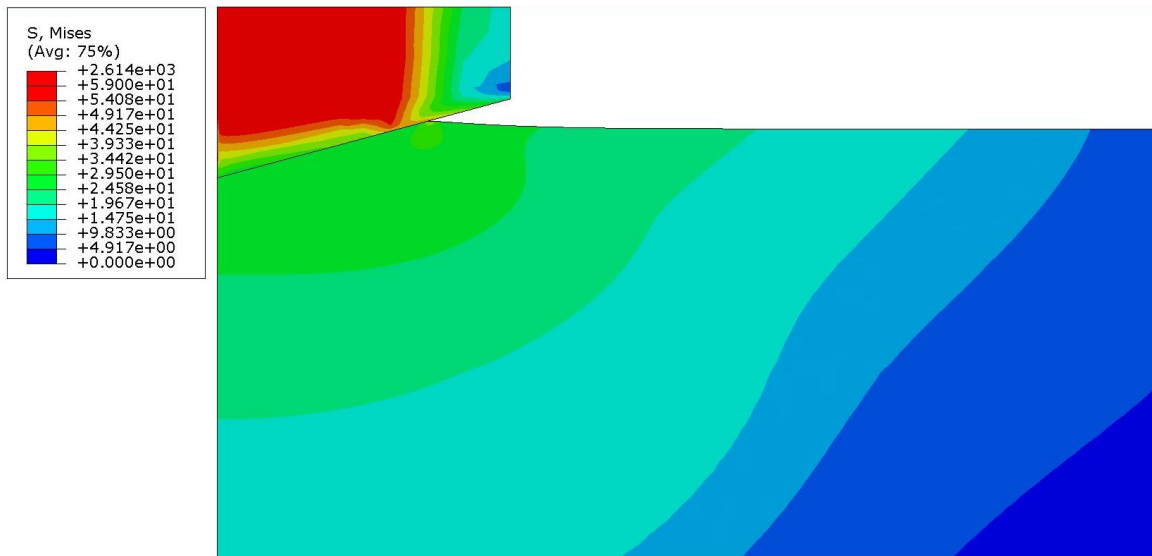


(b)

Figure 20: Contour plots of equivalent creep strain for SnAgCu at 25 °C under indentation strain rates of (a)  $10^{-4}$   $[s^{-1}]$  and (b)  $10^{-7}$   $[s^{-1}]$



(a)



(b)

Figure 21: Contour plots of Von Mises effective stress for SnAgCu at 25 °C under indentation strain rates of (a)  $10^{-4}$   $[s^{-1}]$  and (b)  $10^{-7}$   $[s^{-1}]$

The simulated relationship between indentation strain rate and creep stress is plotted in Figure 22 (solid lines). The dashed lines represent the uniaxial power-law creep relations, based on Ref [24] and used as the model input. Again, the uniaxial power-law creep relations are a direct extension of Figure 3 and are superimposed onto Figure 22 for ease of comparison. From inspection of Figure 22, it is observed that within the range of strain rates prescribed,  $10^{-4} [s^{-1}]$  to  $10^{-7} [s^{-1}]$ , the creep stress values of the four Sn-based materials span from 1.5 to 53 [MPa]. This is marginally different than the creep stress values obtained from the constant load-hold method (Ch. 3). This deviation may be attributed to the higher maximum strain rate of  $10^{-3} [s^{-1}]$  seen in Figure 17, which allows the creep stress to propagate; thus, justifying why the upper limit of the creep stress for the constant load-hold method is slightly higher than that of the constant indentation strain rate method. Amongst their differences, each method does an acceptable job of deriving an  $\dot{\epsilon}_i - \sigma$  relation that is nearly parallel to the uniaxial creep response. This parallel nature enables the stress exponent ( $n$ ) to be calculated as the slope of the indentation derived  $\dot{\epsilon}_i - \sigma$  curve. Table 6 lists the indentation derived stress exponents for the four Sn-based material. The ability to accurately derive the stress exponent through constant strain rate methodology is again validated when comparing Tables 1 & 6. The same holds true when comparing indentation derived creep exponents between constant load-hold (Table 5) and constant strain rate methods.

As mentioned in Chapter 3.1, there is little to no experimental data in the literature investigating the correlation between the creep coefficients (A) obtained from

indentation and uniaxial tests [8,17,19]. Accordingly, this work establishes a metric defined by the ratio of indentation strain rate against uniaxial strain rate ( $\frac{\dot{\epsilon}_s}{\dot{\epsilon}_i}$ ). The calculated strain rate ratios ( $\frac{\dot{\epsilon}_s}{\dot{\epsilon}_i}$ ) are presented in Table 6. A remarkably consistent strain rate ratio of about 0.33 exists in all four Sn-based material models. In practice, one would have to vertically translate the curve to 33% of its strain rate position and would yield the uniaxial creep response of the material. This would only be a valid assumption if the strain rate ratio for all soft metallic systems was approximately 0.33; however, this study alone showed that different indentation creep methods yield marginally different results. When comparing Tables 5-6 it may be determined that Sn at 25 °C, Sn at 120 °C, and SnAgCu at 120 °C all lie within a discrepancy of 9%; whereas, SnAgCu at 25 °C holds the largest discrepancy of 25%. This may be due to the fact that SnAgCu at 25 °C is the hardest of the four materials and the prescribed peak load for the constant load-hold method may have been too small for the model to produce high precision results. Regardless, it is evident that the constant indentation strain rate method produced the most uniform results; accordingly, more material models must be assessed.

Material	$n$	$\dot{\epsilon}_s/\dot{\epsilon}_i$
Sn at 25°C	7.0133	0.332
Sn at 120 °C	7.0062	0.334
SnAgCu at 25 °C	9.8832	0.335
SnAgCu at 120 °C	8.0604	0.335

Table 6: Stress exponent and strain-rate ratio obtained from constant load-hold model

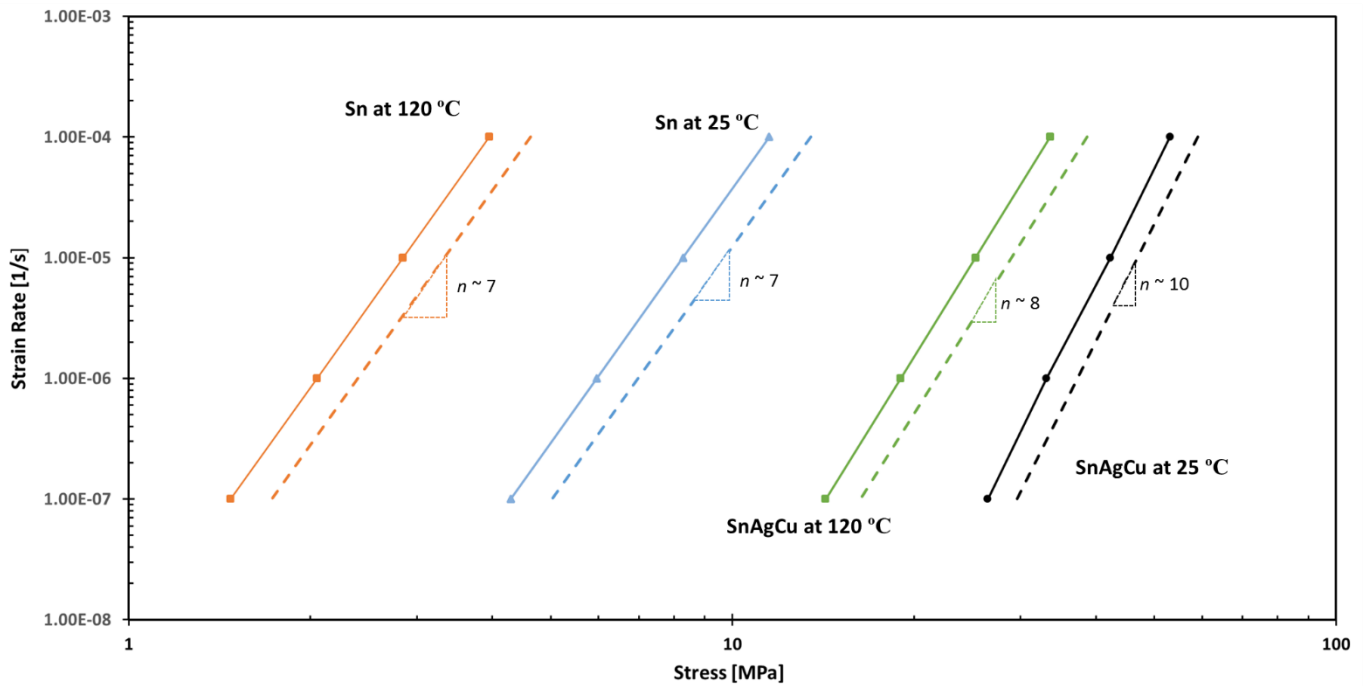


Figure 22: Relationship between indentation strain rate and creep stress, obtained from the indentation modeling (solid lines). The dashed lines represent the power-law creep relations, based on Ref [24] and used as the model input.



## 4.2 – Parametric Analysis (Constant Strain Rate Method)

As mentioned in Section 4.1, a remarkably consistent strain rate ratio of about 0.33 exists in all four Sn-based material models. It was also discovered that this consistent strain rate ratio did not hold true for the constant load-hold method; as the ratio has an increasing trend as the material becomes harder. Accordingly, this raises the question of whether or not the discovered consistent ratio from the constant indentation strain rate method holds true for other soft metallic system. To investigate this problem a parametric analysis was performed where the uniaxial creep stress exponent ( $n$ ) and creep constant ( $A$ ), used as the indentation model input, were varied and the resulting strain rate ratio ( $R = \frac{\dot{\epsilon}_s}{\dot{\epsilon}_i}$ ) was recorded.

The same constant indentation strain rate model used in Section 4.1 is used throughout this parametric analysis with the only varying inputs being the power-law creep parameters. With the exception of the four Sn-based material models, a majority of the material models being investigated are artificially created with varying prescribed power-law creep parameters. A total of 60 simulations were completed, thus, yielding 15  $\dot{\epsilon}_i - \sigma$  relations each with four strain rate conditions. These  $\dot{\epsilon}_i - \sigma$  relations were then used to calculate the ratio between the indentation strain rate and the uniaxial strain rate. These values were monitored for consistency and tabulated in Figure 23 where the strain rate ratio is essentially a function of creep stress exponent ( $n$ ) and creep constant ( $A$ ). Figure 23 displays a basic contour plot where material models with a strain rate ratio of about  $R=0.3$ ,  $0.2$ , and  $0.1$  are displayed as red, green and blue dots,

respectively. It is observed that the ratio (R) is a small value, for material models situated in the extreme-left or lower-left regions of the chart. This means the vertical displacement between the indentation derived response and uniaxial creep response on a  $\dot{\epsilon}_i - \sigma$  plot is significantly larger. One of the most intriguing findings of this analysis is the upper right-hand region of Figure 23. From  $5 \leq n \leq 10$  all of the strain rate ratios are approximately 0.33, with the exception of  $R=0.271$  located at  $n=7$ . The red arc drawn on the plot defines the range of creep parameters needed in order to achieve a strain rate ratio between 0.31 and 0.35.

Figure 23 reveals that, using the constant indentation strain rate method, there appears to be a trend for the strain rate ratio as a result of the combination of A and n. The ratio increases as the combination of A and n moves towards the upper-right region of the chart. There is not a “universal” constant relating the indentation strain rate and uniaxial strain rate. However, if a particular material’s power-law creep parameters fall within the red arc, then we can characterize that materials’ creep response reasonably accurately with  $R \approx 0.33$ . It is also observed that the model can accurately characterize the creep stress exponent (which is also marked in Figure 23) as long as the combination of A and n stays away from the lower-left region of the chart. Figure 23 shows that the model fails to accurately characterize the power-law creep stress exponent (n) for the two cases:  $A = 1.0 \times 10^{-12} \text{ s}^{-1} \text{ MPa}^{-1}$ ,  $n=1$  and  $A = 2.0 \times 10^{-22} \text{ s}^{-1} \text{ MPa}^{-4}$ ,  $n=4$ . These combinations of parameters generally lead to very small creep rates so the materials behave almost elastically until the applied stress becomes exceedingly large. Establishing a domain where the indentation strain rate ratio is known to be constant

will allow for the possibility of vertically translating the curve to R of its strain rate position to yield the uniaxial creep response of the material. Further work may be performed where the contour plot is optimized to a higher resolution.

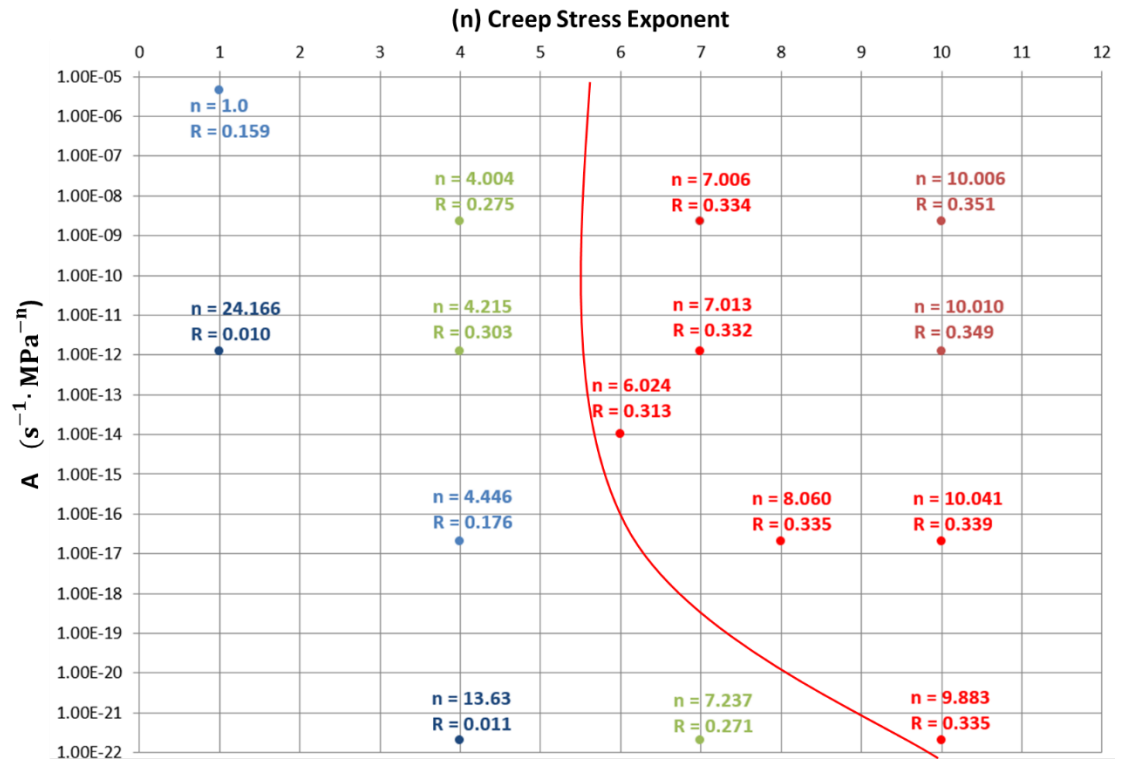


Figure 23: Parametric analysis study – Strain rate ratio values as a function of the creep stress exponent ( $n$ ) and the creep constant ( $A$ );  $(\frac{\dot{\epsilon}_s}{\dot{\epsilon}_t}) = R$

## **Chapter 5: Conclusions and Suggested Future Work**

## 5.1 – Conclusions

Numerical modeling was carried out to investigate the indentation derived creep response using the constant load-hold and constant indentation strain rate methods. The model systems of pure Sn and SnAgCu alloy at two different temperatures were assessed for each indentation technique. The  $\dot{\epsilon}_i - \sigma$  relation for these Sn based materials were compared with their uniaxial counterparts and the difference was quantified. In this work, the average vertical distance between the two curves was calculated and normalized as the ratio of indentation strain rate against uniaxial strain rate ( $\frac{\dot{\epsilon}_s}{\dot{\epsilon}_i}$ ).

The constant load-hold method was assessed for peak loads of 50 $\mu$ N and 100 $\mu$ N. It was discovered that the derived stress exponents ( $n$ ) are independent of peak load and may be accurately obtained through the constant load-hold method. It was also determined that for a specific material under different peak loads, the calculated ratio exhibited reasonable consistency with the largest discrepancy of 6% occurring in SnAgCu at 120 °C. When comparing the ratio of all four Sn-based material models, the value of  $\frac{\dot{\epsilon}_s}{\dot{\epsilon}_i}$  spans from 0.31 to 0.42 with the largest discrepancy of 30% occurring between pure Sn at 120 °C (the weakest material among the four) and SnAgCu at 25 °C (the strongest among the four). There is a tendency of increasing  $\frac{\dot{\epsilon}_s}{\dot{\epsilon}_i}$  as the creep resistance of the material increases.

The constant indentation strain rate method considered indentation strain-rates ( $\dot{\epsilon}_i$ ) ranging from  $10^{-7}$  to  $10^{-4}$  [ $s^{-1}$ ]. By prescribing a constant indentation strain rate, steady-state hardness independent of the indentation depth is obtained. A higher strain rate leads to a higher hardness, and the stress exponents derived from the indentation test are found to be identical to those of their uniaxial counterparts. A remarkably consistent strain rate ratio of about 0.33 exists in all four Sn-based material models. In attempt to further understand the constant strain-rate method, a parametric analysis altering the stress exponent and creep constant was assessed. A distinct trend for the strain rate ratio and creep exponent as a result of the combination of A and n was discovered. The ratio increases as the combination of A and n moves towards the upper-right region of the chart in Figure 23. It was also found that the model fails to accurately characterize the creep exponent when the combination of A and n reside in the bottom-left region of the chart; however, the model is capable of accurately characterizing the creep parameter when the combination of A and n moves toward the upper-right region. There is not a “universal” constant relating the indentation strain rate and uniaxial strain rate. However, if a particular material’s power-law creep parameters fall within the red arc in Figure 23, then we can characterize that materials’ creep response reasonably accurately. In this case the uniaxial creep response ( $\dot{\epsilon}_i - \sigma$  curve) may be determined by vertically translating the curve to 33% of its strain rate position.

## 5.2 – Suggested Future Work

The main objective of this study was to investigate the indentation derived creep response using constant load and constant strain rate methods; however, comparisons between the two methods were limited to the four Sn-based materials. Extending the analysis to cover an extensive range of materials will allow for a more robust comparison of the two instrumented indentation techniques. The suggested study will determine if the perceived trend in this thesis is repeatable.

The constant load-hold method requires several points to be picked along the depth versus time (h-t) curve. As one can imagine, there are countless combinations of points that may be chosen to carry out this analysis. To the best of our knowledge an accepted procedure regarding the point selection has yet been established. It is suggested that a thorough investigation regarding the optimal approach of selecting these points be performed.

Further work may also be extended to the parametric analysis of the constant indentation strain rate method. Although a total of 60 simulations were completed to populate Figure 23 a denser chart is needed to gain a better understanding of the creep behavior for materials of different combinations of A and n.

## References

- [1] Bower, A. F., et al. "Indentation of a power law creeping solid." *Proceedings of the Royal Society of London. Series A: Mathematical and Physical Sciences* 441.1911 (1993): 97-124.
- [2] Su, Caijun, et al. "Measurement of power-law creep parameters by instrumented indentation methods." *Journal of the Mechanics and Physics of Solids* 61.2 (2013): 517-536.
- [3] Shen Y-L. (2010) *Constrained Deformation of Materials*. New York, NY: Springer Science
- [4] Oliver, W. C., and G. M. Pharr. "An improved technique for determining hardness and elastic modulus using load and displacement sensing indentation experiments." *Journal of materials research* 7.06 (1992): 1564-1583.
- [5] Wang, C. L., et al. "Creep of nanocrystalline nickel: A direct comparison between uniaxial and nanoindentation creep." *Scripta Materialia* 62.4 (2010): 175-178.
- [6] Yang, Fuqian, and James CM Li. "Impression test—A review." *Materials Science and Engineering: R: Reports* 74.8 (2013): 233-253.
- [7] Stone, D.S., et al. "Analysis of indentation creep." *Journal of Materials Research* 25.04 (2010): 611-621.
- [8] Lucas, B. N., and W. C. Oliver. "Indentation power-law creep of high-purity indium." *Metallurgical and Materials Transactions A* 30.3 (1999): 601-610.
- [9] Meyers, M.A., and K. K. Chawla. *Mechanical behavior of materials*. Vol. 2. Cambridge: Cambridge university press, 2009.
- [10] Anderson, Robert N. *Materials science*. John Wiley & Sons, Ltd, 1974.
- [11] Hibbeler, R. C. "Mechanics of Materials (2000)."
- [12] Courtney, Thomas H. *Mechanical behavior of materials*. Waveland Press, 2005.
- [13] Cordova, M. E., and Y-L. Shen. "Indentation versus uniaxial power-law creep: a numerical assessment." *Journal of Materials Science* 50.3 (2015): 1394-1400.



- [14] Chu, S. N. G., and J. C. M. Li. "Impression creep; a new creep test." *Journal of Materials Science* 12.11 (1977): 2200-2208.
- [15] Li, James CM. "Impression creep and other localized tests." *Materials Science and Engineering: A* 322.1 (2002): 23-42.
- [16] Takagi, Hidenari, et al. "Experimental and computational creep characterization of Al–Mg solid-solution alloy through instrumented indentation." *Philosophical Magazine* 83.35 (2003): 3959-3976.
- [17] Mayo, M. J., et al. "Mechanical properties of nanophase TiO<sub>2</sub> as determined by nanoindentation." *Journal of Materials Research* 5.05 (1990): 1073-1082.
- [18] Shen, Lu, et al. "Nanoindentation creep of tin and aluminum: A comparative study between constant load and constant strain rate methods." *Materials Science and Engineering: A* 532 (2012): 505-510.
- [19] Raman, V., and R. Berriche. "An investigation of the creep processes in tin and aluminum using a depth-sensing indentation technique." *Journal of materials research* 7.03 (1992): 627-638.
- [20] Goodall, R., and T. W. Clyne. "A critical appraisal of the extraction of creep parameters from nanoindentation data obtained at room temperature." *Acta materialia* 54.20 (2006): 5489-5499.
- [21] Shen, Lu, et al. "Nanoindentation creep of tin and aluminium: A comparative study between constant load and constant strain rate methods." *Materials Science and Engineering: A* 532 (2012): 505-510.
- [22] Shen, Lu, et al. "Creep behaviour of eutectic SnBi alloy and its constituent phases using nanoindentation technique." *Journal of Alloys and Compounds* 574 (2013): 98-103.
- [23] Poisl, W. H., W. C. Oliver, and B. D. Fabes. "The relationship between indentation and uniaxial creep in amorphous selenium." *Journal of materials research* 10.08 (1995): 2024-2032.
- [24] Sidhu, R. S., X. Deng, and N. Chawla. "Microstructure characterization and creep behavior of Pb-free Sn-rich solder alloys: Part II. Creep behavior of bulk solder and solder/copper joints." *Metallurgical and Materials Transactions A* 39.2 (2008): 349-362.

- [25] ABAQUS Version 6.12, Hibbitt Karlsson and Sorenson Inc., Providence, RI, USA, 2010
- [26] Zheng, Hui, et al. "Evaluation of the elastic modulus of thin film considering the substrate effect and geometry effect of indenter tip." *Computational Materials Science* 50.10 (2011): 3026-3031.
- [27] Wei, Yueguang, and John W. Hutchinson. "Hardness trends in micron scale indentation." *Journal of the Mechanics and Physics of Solids* 51.11 (2003): 2037-2056.
- [28] Fisher-Cripps, A. C. "Nanoindentation, 2002."
- [29] Xiao, Gesheng, et al. "Strain rate sensitivity of Sn–3.0 Ag–0.5 Cu solder investigated by nanoindentation." *Materials Science and Engineering: A* 613 (2014): 336-339.

## **Appendix**

## Appendix A – Model Methodology Validation

Almost no experimental work exists which utilizes both the constant load-hold method and constant indentation strain rate method to characterize the creep behavior of the same material. The experimental data presented in Ref [29]; however, included sufficient information for further analysis. Therefore, it was used here as a partial validation of the model methodology. *Xiao et al.* conducted nanoindentation tests with continuous stiffness measurement (CSM) technique on Sn-3.0Ag-0.5Cu lead free solder under different strain rates at room temperature [29]. Constant indentation strain rate condition was realized by performing load-controlled indentations with constant value of loading rate/load ( $\frac{\dot{p}}{p}$ ). Note that  $\frac{\dot{p}}{p} = 2 \dot{\epsilon}_i$  when a steady-state hardness is reached [8].

Representative hardness-depth curves under different  $\frac{\dot{p}}{p}$ , during the loading stage of indentation, were used to derive a  $\dot{\epsilon}_i - \sigma$  relation. Five hardness points and their corresponding  $\frac{\dot{p}}{p}$  values were extracted, and with the use of Equations 2 & 8 the  $\dot{\epsilon}_i - \sigma$  relation was derived. The corresponding  $\dot{\epsilon}_i - \sigma$  curve in Figure 24 is defined as the experimental data at 1500nm of indentation depth (solid blue curve). It was determined that the derived creep exponent held a magnitude of 5.737. The derived  $\dot{\epsilon}_i - \sigma$  relation during the loading stage was then vertically shifted downward 0.33 (See Chapter 4); thus, establishing a uniaxial power-law creep reference (dashed orange curve).

In order to investigate the  $\dot{\epsilon}_i - \sigma$  relation during the holding stage of indentation, creep displacement and indentation strain rate values during the hold period after

loading under different  $\frac{\dot{\epsilon}}{p}$  were extracted from [29]. For various  $\frac{\dot{\epsilon}}{p}$  values of 0.05, 0.1, and  $0.2s^{-1}$ , the corresponding creep exponents obtained from the hold data were 7.379, 6.001, and 6.707, respectively.

It is observed per Figure 24, that two of the  $\dot{\epsilon}_i - \sigma$  curves resulting from the constant load-hold method relatively coincide with the one from the constant indentation strain rate method; however, when  $\frac{\dot{\epsilon}}{p} = 0.2s^{-1}$  the  $\dot{\epsilon}_i - \sigma$  curve resulting from the constant load-hold data deviates towards the uniaxial power-law reference. This deviation may be due to the uncertainty accompanied by approximating the experimental values from [29]. This discrepancy may also be attributed to variations in the experimental setup. Regardless, it has been shown that the creep exponent can roughly be approximated from either the loading or holding period of indentation. The experimental data also demonstrate the less consistent nature of the constant load-hold method in producing the strain rate – stress relationship.

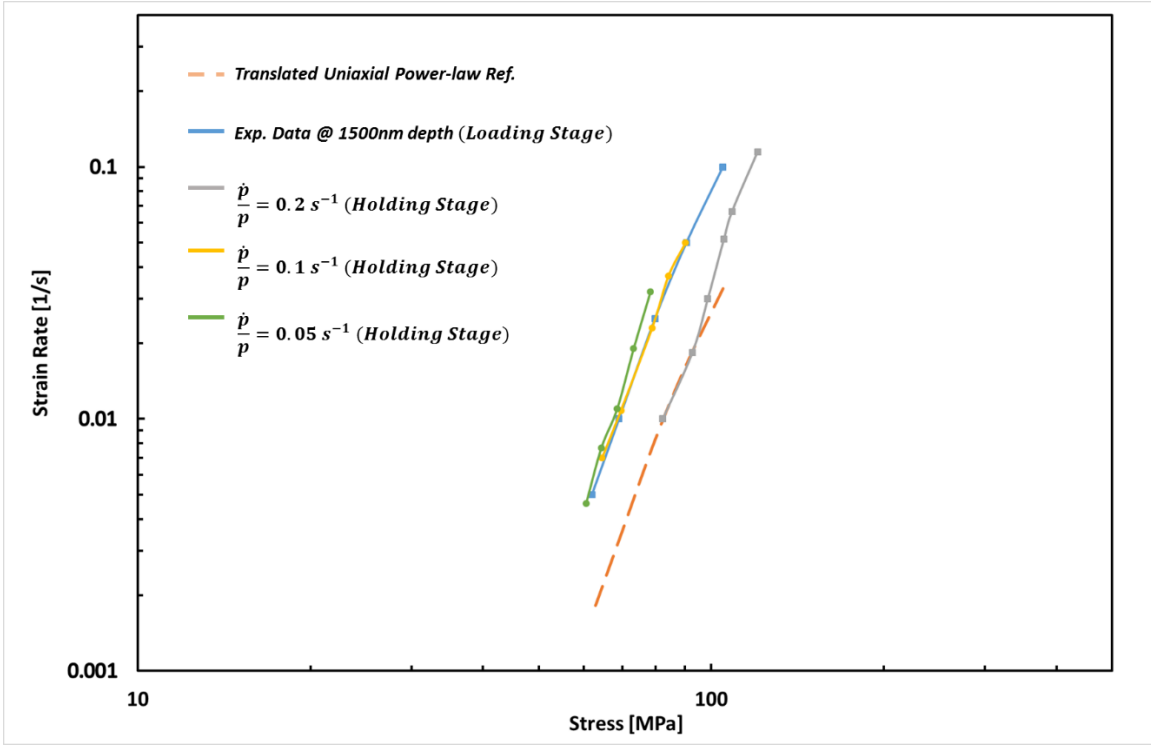


Figure 24: Relationship between indentation strain rate and creep stress, obtained from the experimental data in Ref [29].  $\dot{\epsilon}_i - \sigma$  curves obtained through extraction of experimental data in [29] (solid lines). The dashed line represents the power-law creep relation, based on vertically translating the experimentally derived curve by 0.33.

## Appendix B: Input File – Constant Indentation Strain Rate Method

```
*****
**Constant Indentation Strain Rate Method
**Pure Sn at 120C
**Constant Strain Rate = 1e-7
**
*****
*Heading
Elastic indenter,fric=0.1
*Preprint, echo=no, model=no, history=no
**
**NODE INFORMATION
** Material nodes
*node, nset=left
1, 0.0,0.000
251, 0.0,-0.020
501, 0.0,-0.040
751, 0.0,-0.060
1001, 0.0,-0.080
1251, 0.0,-0.100
1501, 0.0,-0.120
1751, 0.0,-0.140
2001, 0.0,-0.160
2251, 0.0,-0.180
2501, 0.0,-0.200
2751, 0.0,-0.220
3001, 0.0,-0.240
3251, 0.0,-0.260
3501, 0.0,-0.280
3751, 0.0,-0.300
4001, 0.0,-0.320
4251, 0.0,-0.340
4501, 0.0,-0.360
4751, 0.0,-0.380
5001, 0.0,-0.400
5251, 0.0,-0.420
5501, 0.0,-0.440
5751, 0.0,-0.460
6001, 0.0,-0.480
6251, 0.0,-0.500
6501, 0.0,-0.520
6751, 0.0,-0.540
7001, 0.0,-0.560
7251, 0.0,-0.580
7501, 0.0,-0.600
7751, 0.0,-0.620
8001, 0.0,-0.640
8251, 0.0,-0.660
8501, 0.0,-0.680
8751, 0.0,-0.700
9001, 0.0,-0.720
9251, 0.0,-0.740
9501, 0.0,-0.760
9751, 0.0,-0.780
10001, 0.0,-0.800
10251, 0.0,-0.820
```

10501, 0.0,-0.840  
10751, 0.0,-0.860  
11001, 0.0,-0.880  
11251, 0.0,-0.900  
11501, 0.0,-0.920  
11751, 0.0,-0.940  
12001, 0.0,-0.960  
12251, 0.0,-0.980  
12501, 0.0,-1.000  
12751, 0.0,-1.050  
13001, 0.0,-1.100  
13251, 0.0,-1.150  
13501, 0.0,-1.200  
13751, 0.0,-1.250  
14001, 0.0,-1.300  
14251, 0.0,-1.350  
14501, 0.0,-1.400  
14751, 0.0,-1.450  
15001, 0.0,-1.500  
15251, 0.0,-1.550  
15501, 0.0,-1.600  
15751, 0.0,-1.650  
16001, 0.0,-1.700  
16251, 0.0,-1.750  
16501, 0.0,-1.800  
16751, 0.0,-1.850  
17001, 0.0,-1.900  
17251, 0.0,-1.950  
17501, 0.0,-2.000  
17751, 0.0,-2.050  
18001, 0.0,-2.100  
18251, 0.0,-2.150  
18501, 0.0,-2.200  
18751, 0.0,-2.250  
19001, 0.0,-2.300  
19251, 0.0,-2.350  
19501, 0.0,-2.400  
19751, 0.0,-2.450  
20001, 0.0,-2.500  
20251, 0.0,-2.550  
20501, 0.0,-2.600  
20751, 0.0,-2.650  
21001, 0.0,-2.700  
21251, 0.0,-2.750  
21501, 0.0,-2.800  
21751, 0.0,-2.850  
22001, 0.0,-2.900  
22251, 0.0,-2.950  
22501, 0.0,-3.000  
22751, 0.0,-3.050  
23001, 0.0,-3.100  
23251, 0.0,-3.150  
23501, 0.0,-3.200  
23751, 0.0,-3.250  
24001, 0.0,-3.300  
24251, 0.0,-3.350  
24501, 0.0,-3.400  
24751, 0.0,-3.450



25001, 0.0,-3.500  
25251, 0.0,-3.550  
25501, 0.0,-3.600  
25751, 0.0,-3.650  
26001, 0.0,-3.700  
26251, 0.0,-3.750  
26501, 0.0,-3.800  
26751, 0.0,-3.850  
27001, 0.0,-3.900  
27251, 0.0,-3.950  
27501, 0.0,-4.000  
27751, 0.0,-4.050  
28001, 0.0,-4.100  
28251, 0.0,-4.150  
28501, 0.0,-4.200  
28751, 0.0,-4.250  
29001, 0.0,-4.300  
29251, 0.0,-4.350  
29501, 0.0,-4.400  
29751, 0.0,-4.450  
30001, 0.0,-4.500  
30251, 0.0,-4.550  
30501, 0.0,-4.600  
30751, 0.0,-4.650  
31001, 0.0,-4.700  
31251, 0.0,-4.750  
31501, 0.0,-4.800  
31751, 0.0,-4.850  
32001, 0.0,-4.900  
32251, 0.0,-4.950  
32501, 0.0,-5.000  
32751, 0.0,-5.050  
33001, 0.0,-5.100  
33251, 0.0,-5.150  
33501, 0.0,-5.200  
33751, 0.0,-5.250  
34001, 0.0,-5.300  
34251, 0.0,-5.350  
34501, 0.0,-5.400  
34751, 0.0,-5.450  
35001, 0.0,-5.500  
35251, 0.0,-5.550  
35501, 0.0,-5.600  
35751, 0.0,-5.650  
36001, 0.0,-5.700  
36251, 0.0,-5.750  
36501, 0.0,-5.800  
36751, 0.0,-5.850  
37001, 0.0,-5.900  
37251, 0.0,-5.950  
37501, 0.0,-6.000  
37751, 0.0,-6.050  
38001, 0.0,-6.100  
38251, 0.0,-6.150  
38501, 0.0,-6.200  
38751, 0.0,-6.250  
39001, 0.0,-6.300  
39251, 0.0,-6.350

39501, 0.0,-6.400  
39751, 0.0,-6.450  
40001, 0.0,-6.500  
40251, 0.0,-6.550  
40501, 0.0,-6.600  
40751, 0.0,-6.650  
41001, 0.0,-6.700  
41251, 0.0,-6.750  
41501, 0.0,-6.800  
41751, 0.0,-6.850  
42001, 0.0,-6.900  
42251, 0.0,-6.950  
42501, 0.0,-7.000  
42751, 0.0,-7.050  
43001, 0.0,-7.100  
43251, 0.0,-7.150  
43501, 0.0,-7.200  
43751, 0.0,-7.250  
44001, 0.0,-7.300  
44251, 0.0,-7.350  
44501, 0.0,-7.400  
44751, 0.0,-7.450  
45001, 0.0,-7.500  
45251, 0.0,-7.600  
45501, 0.0,-7.700  
45751, 0.0,-7.800  
46001, 0.0,-7.900  
46251, 0.0,-8.000  
46501, 0.0,-8.100  
46751, 0.0,-8.200  
47001, 0.0,-8.300  
47251, 0.0,-8.400  
47501, 0.0,-8.500  
47751, 0.0,-8.600  
48001, 0.0,-8.700  
48251, 0.0,-8.800  
48501, 0.0,-8.900  
48751, 0.0,-9.000  
49001, 0.0,-9.100  
49251, 0.0,-9.200  
49501, 0.0,-9.300  
49751, 0.0,-9.400  
50001, 0.0,-9.500  
50251, 0.0,-9.600  
50501, 0.0,-9.700  
50751, 0.0,-9.800  
51001, 0.0,-9.900  
51251, 0.0,-10.000  
51501, 0.0,-10.200  
51751, 0.0,-10.500  
52001, 0.0,-11.000  
52251, 0.0,-12.000  
52501, 0.0,-13.000  
52751, 0.0,-14.000  
53001, 0.0,-15.000  
53251, 0.0,-16.000  
53501, 0.0,-17.000  
53751, 0.0,-18.000

54001, 0.0,-19.000  
54251, 0.0,-20.000  
54501, 0.0,-22.000  
54751, 0.0,-24.000  
55001, 0.0,-26.000  
55251, 0.0,-28.000  
55501, 0.0,-30.000  
55751, 0.0,-32.000  
56001, 0.0,-34.000  
56251, 0.0,-36.000  
56501, 0.0,-38.000  
56751, 0.0,-40.000  
57001, 0.0,-42.000  
57251, 0.0,-44.000  
57501, 0.0,-46.000  
57751, 0.0,-48.000  
58001, 0.0,-50.000  
58251, 0.0,-55.000  
58501, 0.0,-60.000  
58751, 0.0,-65.000  
59001, 0.0,-70.000  
59251, 0.0,-75.000  
59501, 0.0,-80.000  
59751, 0.0,-90.000  
60001, 0.0,-100.000  
60251, 0.0,-120.000  
60501, 0.0,-160.000  
60751, 0.0,-200.000  
\*node, nset=right  
250, 200.0,0.000  
500, 200.0,-0.020  
750, 200.0,-0.040  
1000, 200.0,-0.060  
1250, 200.0,-0.080  
1500, 200.0,-0.100  
1750, 200.0,-0.120  
2000, 200.0,-0.140  
2250, 200.0,-0.160  
2500, 200.0,-0.180  
2750, 200.0,-0.200  
3000, 200.0,-0.220  
3250, 200.0,-0.240  
3500, 200.0,-0.260  
3750, 200.0,-0.280  
4000, 200.0,-0.300  
4250, 200.0,-0.320  
4500, 200.0,-0.340  
4750, 200.0,-0.360  
5000, 200.0,-0.380  
5250, 200.0,-0.400  
5500, 200.0,-0.420  
5750, 200.0,-0.440  
6000, 200.0,-0.460  
6250, 200.0,-0.480  
6500, 200.0,-0.500  
6750, 200.0,-0.520  
7000, 200.0,-0.540  
7250, 200.0,-0.560

7500, 200.0,-0.580  
7750, 200.0,-0.600  
8000, 200.0,-0.620  
8250, 200.0,-0.640  
8500, 200.0,-0.660  
8750, 200.0,-0.680  
9000, 200.0,-0.700  
9250, 200.0,-0.720  
9500, 200.0,-0.740  
9750, 200.0,-0.760  
10000, 200.0,-0.780  
10250, 200.0,-0.800  
10500, 200.0,-0.820  
10750, 200.0,-0.840  
11000, 200.0,-0.860  
11250, 200.0,-0.880  
11500, 200.0,-0.900  
11750, 200.0,-0.920  
12000, 200.0,-0.940  
12250, 200.0,-0.960  
12500, 200.0,-0.980  
12750, 200.0,-1.000  
13000, 200.0,-1.050  
13250, 200.0,-1.100  
13500, 200.0,-1.150  
13750, 200.0,-1.200  
14000, 200.0,-1.250  
14250, 200.0,-1.300  
14500, 200.0,-1.350  
14750, 200.0,-1.400  
15000, 200.0,-1.450  
15250, 200.0,-1.500  
15500, 200.0,-1.550  
15750, 200.0,-1.600  
16000, 200.0,-1.650  
16250, 200.0,-1.700  
16500, 200.0,-1.750  
16750, 200.0,-1.800  
17000, 200.0,-1.850  
17250, 200.0,-1.900  
17500, 200.0,-1.950  
17750, 200.0,-2.000  
18000, 200.0,-2.050  
18250, 200.0,-2.100  
18500, 200.0,-2.150  
18750, 200.0,-2.200  
19000, 200.0,-2.250  
19250, 200.0,-2.300  
19500, 200.0,-2.350  
19750, 200.0,-2.400  
20000, 200.0,-2.450  
20250, 200.0,-2.500  
20500, 200.0,-2.550  
20750, 200.0,-2.600  
21000, 200.0,-2.650  
21250, 200.0,-2.700  
21500, 200.0,-2.750  
21750, 200.0,-2.800

22000, 200.0,-2.850  
22250, 200.0,-2.900  
22500, 200.0,-2.950  
22750, 200.0,-3.000  
23000, 200.0,-3.050  
23250, 200.0,-3.100  
23500, 200.0,-3.150  
23750, 200.0,-3.200  
24000, 200.0,-3.250  
24250, 200.0,-3.300  
24500, 200.0,-3.350  
24750, 200.0,-3.400  
25000, 200.0,-3.450  
25250, 200.0,-3.500  
25500, 200.0,-3.550  
25750, 200.0,-3.600  
26000, 200.0,-3.650  
26250, 200.0,-3.700  
26500, 200.0,-3.750  
26750, 200.0,-3.800  
27000, 200.0,-3.850  
27250, 200.0,-3.900  
27500, 200.0,-3.950  
27750, 200.0,-4.000  
28000, 200.0,-4.050  
28250, 200.0,-4.100  
28500, 200.0,-4.150  
28750, 200.0,-4.200  
29000, 200.0,-4.250  
29250, 200.0,-4.300  
29500, 200.0,-4.350  
29750, 200.0,-4.400  
30000, 200.0,-4.450  
30250, 200.0,-4.500  
30500, 200.0,-4.550  
30750, 200.0,-4.600  
31000, 200.0,-4.650  
31250, 200.0,-4.700  
31500, 200.0,-4.750  
31750, 200.0,-4.800  
32000, 200.0,-4.850  
32250, 200.0,-4.900  
32500, 200.0,-4.950  
32750, 200.0,-5.000  
33000, 200.0,-5.050  
33250, 200.0,-5.100  
33500, 200.0,-5.150  
33750, 200.0,-5.200  
34000, 200.0,-5.250  
34250, 200.0,-5.300  
34500, 200.0,-5.350  
34750, 200.0,-5.400  
35000, 200.0,-5.450  
35250, 200.0,-5.500  
35500, 200.0,-5.550  
35750, 200.0,-5.600  
36000, 200.0,-5.650  
36250, 200.0,-5.700

36500, 200.0, -5.750  
36750, 200.0, -5.800  
37000, 200.0, -5.850  
37250, 200.0, -5.900  
37500, 200.0, -5.950  
37750, 200.0, -6.000  
38000, 200.0, -6.050  
38250, 200.0, -6.100  
38500, 200.0, -6.150  
38750, 200.0, -6.200  
39000, 200.0, -6.250  
39250, 200.0, -6.300  
39500, 200.0, -6.350  
39750, 200.0, -6.400  
40000, 200.0, -6.450  
40250, 200.0, -6.500  
40500, 200.0, -6.550  
40750, 200.0, -6.600  
41000, 200.0, -6.650  
41250, 200.0, -6.700  
41500, 200.0, -6.750  
41750, 200.0, -6.800  
42000, 200.0, -6.850  
42250, 200.0, -6.900  
42500, 200.0, -6.950  
42750, 200.0, -7.000  
43000, 200.0, -7.050  
43250, 200.0, -7.100  
43500, 200.0, -7.150  
43750, 200.0, -7.200  
44000, 200.0, -7.250  
44250, 200.0, -7.300  
44500, 200.0, -7.350  
44750, 200.0, -7.400  
45000, 200.0, -7.450  
45250, 200.0, -7.500  
45500, 200.0, -7.600  
45750, 200.0, -7.700  
46000, 200.0, -7.800  
46250, 200.0, -7.900  
46500, 200.0, -8.000  
46750, 200.0, -8.100  
47000, 200.0, -8.200  
47250, 200.0, -8.300  
47500, 200.0, -8.400  
47750, 200.0, -8.500  
48000, 200.0, -8.600  
48250, 200.0, -8.700  
48500, 200.0, -8.800  
48750, 200.0, -8.900  
49000, 200.0, -9.000  
49250, 200.0, -9.100  
49500, 200.0, -9.200  
49750, 200.0, -9.300  
50000, 200.0, -9.400  
50250, 200.0, -9.500  
50500, 200.0, -9.600  
50750, 200.0, -9.700

```

51000, 200.0,-9.800
51250, 200.0,-9.900
51500, 200.0,-10.000
51750, 200.0,-10.200
52000, 200.0,-10.500
52250, 200.0,-11.000
52500, 200.0,-12.000
52750, 200.0,-13.000
53000, 200.0,-14.000
53250, 200.0,-15.000
53500, 200.0,-16.000
53750, 200.0,-17.000
54000, 200.0,-18.000
54250, 200.0,-19.000
54500, 200.0,-20.000
54750, 200.0,-22.000
55000, 200.0,-24.000
55250, 200.0,-26.000
55500, 200.0,-28.000
55750, 200.0,-30.000
56000, 200.0,-32.000
56250, 200.0,-34.000
56500, 200.0,-36.000
56750, 200.0,-38.000
57000, 200.0,-40.000
57250, 200.0,-42.000
57500, 200.0,-44.000
57750, 200.0,-46.000
58000, 200.0,-48.000
58250, 200.0,-50.000
58500, 200.0,-55.000
58750, 200.0,-60.000
59000, 200.0,-65.000
59250, 200.0,-70.000
59500, 200.0,-75.000
59750, 200.0,-80.000
60000, 200.0,-90.000
60250, 200.0,-100.000
60500, 200.0,-120.000
60750, 200.0,-160.000
61000, 200.0,-200.000
*nset, nset=bottom, generate
60751, 61000, 1
*nset, nset=top, generate
1, 250, 1
**nset, nset=internal, generate
**123,118623,250
** "normal" bias: 0.973, use 0.97 to test shallow indentation
*nfill, bias=0.976
left, right, 249, 1
**nfill, bias=0.6
**internal,right ,127,1
**
** indenter nodes
*node, nset=ind-left
1141001, 0.0, 0.0003
1141032, 0.0, 0.003
1141063, 0.0, 0.006

```

1141094, 0.0,	0.009
1141125, 0.0,	0.015
1141156, 0.0,	0.021
1141187, 0.0,	0.027
1141218, 0.0,	0.036
1141249, 0.0,	0.045
1141280, 0.0,	0.054
1141311, 0.0,	0.063
1141342, 0.0,	0.075
1141373, 0.0,	0.087
1141404, 0.0,	0.099
1141435, 0.0,	0.111
1141466, 0.0,	0.123
1141497, 0.0,	0.141
1141528, 0.0,	0.165
1141559, 0.0,	0.18
1141590, 0.0,	0.24
1141621, 0.0,	0.3
1141652, 0.0,	0.45
1141683, 0.0,	0.6
1141714, 0.0,	0.75
1141745, 0.0,	0.9
1141776, 0.0,	1.05
1141807, 0.0,	1.2
1141838, 0.0,	1.35
1141869, 0.0,	4
1141900, 0.0,	9
1141931, 0.0,	14
*node, nset=ind-righ	
1141031, 18.0,	6.45
1141062, 18.0,	6.451
1141093, 18.0,	6.452
1141124, 18.0,	6.453
1141155, 18.0,	6.454
1141186, 18.0,	6.455
1141217, 18.0,	6.456
1141248, 18.0,	6.457
1141279, 18.0,	6.458
1141310, 18.0,	6.459
1141341, 18.0,	6.46
1141372, 18.0,	6.461
1141403, 18.0,	6.462
1141434, 18.0,	6.463
1141465, 18.0,	6.563
1141496, 18.0,	6.663
1141527, 18.0,	6.763
1141558, 18.0,	6.863
1141589, 18.0,	6.963
1141620, 18.0,	7
1141651, 18.0,	7.1
1141682, 18.0,	7.2
1141713, 18.0,	7.3
1141744, 18.0,	7.4
1141775, 18.0,	7.5
1141806, 18.0,	7.6
1141837, 18.0,	7.7
1141868, 18.0,	7.8
1141899, 18.0,	7.9



```

1141930, 18.0, 10
1141961, 18.0, 14
*nfill, bias=0.84
ind-left, ind-right, 30, 1
*nset, nset=ind-all, generate
1141001, 1141961, 1
*nset, nset=ind-top, generate
1141931, 1141961, 1
*nset, nset=ind-bot, generate
1141001, 1141031, 1
*nset, nset=ind-tip
1141961
*nset, nset=indtop-1, generate
1141931, 1141960, 1
*nset, nset=All, generate
1,180000,1,
**
**
**ELEMENT INFORMATION
**
*Element, type=CAX4
1, 251, 252, 2, 1
*elgen, elset=whole
1, 249, 1, 1, 243, 250, 249
**elset, elset=film, generate
**1, 11940, 1
*elset, elset=up_film, generate
1, 700, 1
*elset, elset=low_film, generate
701,42330, 1
*elset, elset=sub, generate
42331, 60507, 1
**
*Elset, elset=Set-1, generate
1, 200, 1
**
*Elset, elset=__PickedSurf7_S3, generate
1, 200, 1
**
*element, type=cax4
1141001, 1141001, 1141002, 1141033, 1141032
*elgen, elset=indenter
1141001, 30, 1, 1, 30, 31, 30
*elset, elset=ind_bot_ele, generate
1141001, 1141030, 1
**
*surface, name=indsurf
ind_bot_ele, s1
**
*Surface, name=_PickedSurf7
__PickedSurf7_S3, S3
*Contact Pair, interaction=IntProp-1
__PickedSurf7, indsurf
*Surface Interaction, name=IntProp-1
*Friction
0.1
**
*solid section, elset=up_film, material=sn

```

```

*solid section, elset=low_film, material=sn
*solid section, elset=sub, material=sn
*Solid Section, elset=indenter, material=diamond
**
*material, name=diamond
*elastic
1141000.0, 0.07
**
*MATERIAL, NAME=sn
*ELASTIC
35000.0, 0.34
**Plastic
**1.9, 0.0
*Expansion
24e-6
*creep, law=strain
2.20E-9,7.0,0.0,120.0
**
*material, name=Si
*elastic
130000.0, 0.28
*Expansion
3.0e-6
**
*Material, name=cu
*elastic
110000.0, 0.3
*plastic
155.0, 0.0
*Expansion
3.0e-6
*Material, name=SiO2
*elastic
71400.0, 0.16
*plastic
3500.0, 0.0
**
*Initial conditions,Type=Temperature
All,20
**BOUNDARY CONDITIONS
*EQUATION
2
indtop-1, 2, 1.0, 1141961, 2, -1.0
**
*Boundary
Left, 1
Bottom, 2
ind-left, 1
**
**
*RESTART,WRITE,OVERLAY
** -----
**
**
** STEP: Step-1
**
*Step, INC=600000, NLGEOM=YES, UNSYMM=YES
**static

```

```

*visco, cetol=0.0005
1000.0, 10000000.0, 0.0005, 100000.0
**
*CONTROLS, ANALYSIS=DISCONTINUOUS
*CONTROLS, PARAMETERS=LINE SEARCH
4,4,0.25,0.25,0.15
** BOUNDARY CONDITIONS
**
*Boundary
ind-tip, 2, 2, -0.4
**
** OUTPUT REQUESTS
*OUTPUT, FIELD, frequency=1000
*ELEMENT OUTPUT
S, MISES, E, CEEQ
*node output
u
*CONTACT OUTPUT, VARIABLE=PRESELECT, NSET=top
*OUTPUT, HISTORY, variables=preselect, frequency=1
*NODE OUTPUT, NSET=ind-tip
u2, rf2
*NODE OUTPUT, NSET=top
COORD
*NODE print, NSET=ind-tip, frequency=1
U, RF2
*node print, nset=top, frequency=50000
coord, U, RF2
*End Step
**
**
** STEP: Step-2
**
*Step, INC=600000, NLGEOM=YES, UNSYMM=YES
**static
*visco, cetol=0.0005
1000.0, 5000000.0, 0.0005, 50000.0
**
*CONTROLS, ANALYSIS=DISCONTINUOUS
*CONTROLS, PARAMETERS=LINE SEARCH
4,4,0.25,0.25,0.15
** BOUNDARY CONDITIONS
**
*Boundary
ind-tip, 2, 2, -0.8
**
** OUTPUT REQUESTS
*OUTPUT, FIELD, frequency=1000
*ELEMENT OUTPUT
S, MISES, E, CEEQ
*node output
u
*CONTACT OUTPUT, VARIABLE=PRESELECT, NSET=top
*OUTPUT, HISTORY, variables=preselect, frequency=1
*NODE OUTPUT, NSET=ind-tip
u2, rf2
*NODE OUTPUT, NSET=top
COORD
*NODE print, NSET=ind-tip, frequency=1

```

```

U,RF2
*node print, nset=top,frequency=50000
coord, U, RF2
*End Step
**
** STEP: Step-3
**
*Step, INC=600000, NLGEOM=YES, UNSYMM=YES
**static
*visco, cetol=0.0005
1000.0, 3333333.3, 0.0005, 33333.3
**
*CONTROLS, ANALYSIS=DISCONTINUOUS
*CONTROLS, PARAMETERS=LINE SEARCH
4,4,0.25,0.25,0.15
** BOUNDARY CONDITIONS
**
*Boundary
ind-tip, 2, 2, -1.2
**
** OUTPUT REQUESTS
*OUTPUT,FIELD,frequency=1000
*ELEMENT OUTPUT
S,MISES,E,CEEQ
*node output
u
*CONTACT OUTPUT,VARIABLE=PRESELECT,NSET=top
*OUTPUT,HISTORY,variables=preselect, frequency=1
*NODE OUTPUT,NSET=ind-tip
u2, rf2
*NODE OUTPUT, NSET=top
COORD
*NODE print,NSET=ind-tip,frequency=1
U,RF2
*node print, nset=top,frequency=50000
coord, U, RF2
*End Step
**
** STEP: Step-4
**
*Step, INC=600000, NLGEOM=YES, UNSYMM=YES
**static
*visco, cetol=0.0005
1000.0, 2500000.0, 0.0005, 25000.0
**
*CONTROLS, ANALYSIS=DISCONTINUOUS
*CONTROLS, PARAMETERS=LINE SEARCH
4,4,0.25,0.25,0.15
** BOUNDARY CONDITIONS
**
*Boundary
ind-tip, 2, 2, -1.6
**
** OUTPUT REQUESTS
*OUTPUT,FIELD,frequency=1000
*ELEMENT OUTPUT
S,MISES,E,CEEQ
*node output

```

```

u
*CONTACT OUTPUT,VARIABLE=PRESELECT,NSET=top
*OUTPUT,HISTORY,variables=preselect, frequency=1
*NODE OUTPUT,NSET=ind-tip
u2, rf2
*NODE OUTPUT, NSET=top
COORD
*NODE print,NSET=ind-tip,frequency=1
U,RF2
*node print, nset=top,frequency=50000
coord, U, RF2
*End Step
**
** STEP: Step-5
**
*Step, INC=600000, NLGEOM=YES, UNSYMM=YES
**static
*visco, cetol=0.0005
1000.0, 2000000.0, 0.0005, 20000.0
**
*CONTROLS, ANALYSIS=DISCONTINUOUS
*CONTROLS, PARAMETERS=LINE SEARCH
4,4,0.25,0.25,0.15
** BOUNDARY CONDITIONS
**
*Boundary
ind-tip, 2, 2, -2.0
**
** OUTPUT REQUESTS
*OUTPUT,FIELD,frequency=1000
*ELEMENT OUTPUT
S,MISES,E,CEEQ
*node output
u
*CONTACT OUTPUT,VARIABLE=PRESELECT,NSET=top
*OUTPUT,HISTORY,variables=preselect, frequency=1
*NODE OUTPUT,NSET=ind-tip
u2, rf2
*NODE OUTPUT, NSET=top
COORD
*NODE print,NSET=ind-tip,frequency=1
U,RF2
*node print, nset=top,frequency=50000
coord, U, RF2
*End Step
**
** STEP: Step-6
**
*Step, INC=600000, NLGEOM=YES, UNSYMM=YES
**static
*visco, cetol=0.0005
1000.0, 1666666.6, 0.0005, 16666.6
**
*CONTROLS, ANALYSIS=DISCONTINUOUS
*CONTROLS, PARAMETERS=LINE SEARCH
4,4,0.25,0.25,0.15
** BOUNDARY CONDITIONS
**

```

```

*Boundary
ind-tip, 2, 2, -2.4
**
** OUTPUT REQUESTS
*OUTPUT,FIELD,frequency=1000
*ELEMENT OUTPUT
S,MISES,E,CEEQ
*node output
u
*CONTACT OUTPUT,VARIABLE=PRESELECT,NSET=top
*OUTPUT,HISTORY,variables=preselect, frequency=1
*NODE OUTPUT,NSET=ind-tip
u2, rf2
*NODE OUTPUT, NSET=top
COORD
*NODE print,NSET=ind-tip,frequency=1
U,RF2
*node print, nset=top,frequency=50000
coord, U, RF2
*End Step
**
** STEP: Step-7
**
*Step, INC=600000, NLGEOM=YES, UNSYMM=YES
**static
*visco, cetol=0.0005
1000.0, 1428571.0, 0.0005, 14285.0
**
*CONTROLS, ANALYSIS=DISCONTINUOUS
*CONTROLS, PARAMETERS=LINE SEARCH
4,4,0.25,0.25,0.15
** BOUNDARY CONDITIONS
**
*Boundary
ind-tip, 2, 2, -2.8
**
** OUTPUT REQUESTS
*OUTPUT,FIELD,frequency=1000
*ELEMENT OUTPUT
S,MISES,E,CEEQ
*node output
u
*CONTACT OUTPUT,VARIABLE=PRESELECT,NSET=top
*OUTPUT,HISTORY,variables=preselect, frequency=1
*NODE OUTPUT,NSET=ind-tip
u2, rf2
*NODE OUTPUT, NSET=top
COORD
*NODE print,NSET=ind-tip,frequency=1
U,RF2
*node print, nset=top,frequency=50000
coord, U, RF2
*End Step
**
** STEP: Step-8
**
*Step, INC=600000, NLGEOM=YES, UNSYMM=YES
**static

```

```

*visco, cetol=0.0005
1000.0, 1250000.0, 0.0005, 12500.0
**
*CONTROLS, ANALYSIS=DISCONTINUOUS
*CONTROLS, PARAMETERS=LINE SEARCH
4,4,0.25,0.25,0.15
** BOUNDARY CONDITIONS
**
*Boundary
ind-tip, 2, 2, -3.2
**
** OUTPUT REQUESTS
*OUTPUT, FIELD, frequency=1000
*ELEMENT OUTPUT
S, MISES, E, CEEQ
*node output
u
*CONTACT OUTPUT, VARIABLE=PRESELECT, NSET=top
*OUTPUT, HISTORY, variables=preselect, frequency=1
*NODE OUTPUT, NSET=ind-tip
u2, rf2
*NODE OUTPUT, NSET=top
COORD
*NODE print, NSET=ind-tip, frequency=1
U, RF2
*node print, nset=top, frequency=50000
coord, U, RF2
*End Step
**
** STEP: Step-9
**
*Step, INC=600000, NLGEOM=YES, UNSYMM=YES
**static
*visco, cetol=0.0005
1000.0, 1111111.1, 0.0005, 11111.1
**
*CONTROLS, ANALYSIS=DISCONTINUOUS
*CONTROLS, PARAMETERS=LINE SEARCH
4,4,0.25,0.25,0.15
** BOUNDARY CONDITIONS
**
*Boundary
ind-tip, 2, 2, -3.6
**
** OUTPUT REQUESTS
*OUTPUT, FIELD, frequency=1000
*ELEMENT OUTPUT
S, MISES, E, CEEQ
*node output
u
*CONTACT OUTPUT, VARIABLE=PRESELECT, NSET=top
*OUTPUT, HISTORY, variables=preselect, frequency=1
*NODE OUTPUT, NSET=ind-tip
u2, rf2
*NODE OUTPUT, NSET=top
COORD
*NODE print, NSET=ind-tip, frequency=1
U, RF2

```

```

*node print, nset=top,frequency=50000
coord, U, RF2
*End Step
**
** STEP: Step-10
**
*Step, INC=600000, NLGEOM=YES, UNSYMM=YES
**static
*visco, cetol=0.0005
1000.0, 1000000.0, 0.0005, 10000.0
**
*CONTROLS, ANALYSIS=DISCONTINUOUS
*CONTROLS, PARAMETERS=LINE SEARCH
4,4,0.25,0.25,0.15
** BOUNDARY CONDITIONS
**
*Boundary
ind-tip, 2, 2, -4.0
**
** OUTPUT REQUESTS
*OUTPUT,FIELD,frequency=1000
*ELEMENT OUTPUT
S,MISES,E,CEEQ
*node output
u
*CONTACT OUTPUT,VARIABLE=PRESELECT,NSET=top
*OUTPUT,HISTORY,variables=preselect, frequency=1
*NODE OUTPUT,NSET=ind-tip
u2, rf2
*NODE OUTPUT, NSET=top
COORD
*NODE print,NSET=ind-tip,frequency=1
U,RF2
*node print, nset=top,frequency=50000
coord, U, RF2
*End Step
**
** STEP: Step-unload
**
*Step, INC=600000, NLGEOM=YES, UNSYMM=YES
**static
*visco, cetol=0.0005
0.05, 1000000.0, 0.0005, 10.0
**
*CONTROLS, ANALYSIS=DISCONTINUOUS
*CONTROLS, PARAMETERS=LINE SEARCH
4,4,0.25,0.25,0.15
** BOUNDARY CONDITIONS
**
*Boundary
ind-tip, 2, 2, 0.0
**
** OUTPUT REQUESTS
*OUTPUT,FIELD,frequency=10000
*ELEMENT OUTPUT
S,MISES,E,CEEQ
*node output
u

```



```
*OUTPUT,HISTORY,variables=preselect, frequency=1
*CONTACT OUTPUT,VARIABLE=PRESELECT,NSET=top
*NODE OUTPUT,NSET=ind-tip
u2, rf2
*NODE OUTPUT, NSET=top
COORD
*NODE print,NSET=ind-tip,frequency=1
U,RF2
*node print, nset=top,frequency=50000
coord, U, RF2
*End Step
**
```

## Appendix C: Input File - Constant Load-Hold Method

```
*****
**Constant Load-Hold Method
**Pure Sn at 25C
**Constant load = 100 uN
**
*****
*Heading
** Job name: 100uN_Sn25_30hrs Model name: test
** Generated by: Abaqus/CAE 6.12-1
**Preprint, echo=NO, model=NO, history=NO, contact=NO
**
** PARTS
**
*Part, name=BSURF
*End Part
**
*Part, name=PART-1
*Node
  1, 0., 0.
  2, 0.0116365002, 0.
  3, 0.0235591438, 0.
  4, 0.0357749686, 0.
  5, 0.0482911803, 0.
  6, 0.061115168, 0.
  7, 0.0742544979, 0.
  8, 0.0877169296, 0.
  9, 0.101510406, 0.
  10, 0.115643062, 0.
  11, 0.130123243, 0.
  12, 0.144959494, 0.
  13, 0.160160571, 0.
  14, 0.175735444, 0.
  15, 0.191693321, 0.
  16, 0.20804359, 0.
  17, 0.224795908, 0.
  18, 0.241960183, 0.
  19, 0.259546518, 0.
  20, 0.2775653, 0.
  21, 0.296027184, 0.
  22, 0.314943045, 0.
  23, 0.334324062, 0.
  24, 0.354181617, 0.
  25, 0.374527514, 0.
  26, 0.395373702, 0.
  27, 0.41673252, 0.
  28, 0.438616544, 0.
  29, 0.461038679, 0.
  30, 0.484012216, 0.
  31, 0.507550657, 0.
  32, 0.531667888, 0.
  33, 0.556378186, 0.
  34, 0.581696153, 0.
  35, 0.607636631, 0.
  36, 0.634214997, 0.
  37, 0.661446989, 0.
```

38, 0.689348578,	0.
39, 0.717936277,	0.
40, 0.747226954,	0.
41, 0.777237833,	0.
42, 0.807986736,	0.
43, 0.839491785,	0.
44, 0.871771514,	0.
45, 0.904845059,	0.
46, 0.938731849,	0.
47, 0.973451912,	0.
48, 1.00902569,	0.
49, 1.04547429,	0.
50, 1.08281922,	0
.	
.	
.	
60950, 59.0309296,	-200.
60951, 60.4941483,	-200.
60952, 61.9933434,	-200.
60953, 63.5294075,	-200.
60954, 65.103241,	-200.
60955, 66.7157822,	-200.
60956, 68.3679657,	-200.
60957, 70.0607834,	-200.
60958, 71.7952271,	-200.
60959, 73.572319,	-200.
60960, 75.3931122,	-200.
60961, 77.2586746,	-200.
60962, 79.1701126,	-200.
60963, 81.1285553,	-200.
60964, 83.1351624,	-200.
60965, 85.1911011,	-200.
60966, 87.2975998,	-200.
60967, 89.4559021,	-200.
60968, 91.6672745,	-200.
60969, 93.9330215,	-200.
60970, 96.2544861,	-200.
60971, 98.6330414,	-200.
60972, 101.070076,	-200.
60973, 103.567047,	-200.
60974, 106.125412,	-200.
60975, 108.746689,	-200.
60976, 111.432426,	-200.
60977, 114.184204,	-200.
60978, 117.003647,	-200.
60979, 119.892426,	-200.
60980, 122.852234,	-200.
60981, 125.884827,	-200.
60982, 128.991989,	-200.
60983, 132.175568,	-200.
60984, 135.437424,	-200.
60985, 138.77948,	-200.
60986, 142.203735,	-200.
60987, 145.712173,	-200.
60988, 149.3069,	-200.
60989, 152.990021,	-200.
60990, 156.763702,	-200.
60991, 160.630188,	-200.

60992, 164.591751, -200.  
60993, 168.650726, -200.  
60994, 172.809509, -200.  
60995, 177.070557, -200.  
60996, 181.436386, -200.  
60997, 185.909576, -200.  
60998, 190.492752, -200.  
60999, 195.188644, -200.  
61000, 200., -200.

\*Element, type=CAX4

1, 251, 252, 2, 1  
2, 252, 253, 3, 2  
3, 253, 254, 4, 3  
4, 254, 255, 5, 4  
5, 255, 256, 6, 5  
6, 256, 257, 7, 6  
7, 257, 258, 8, 7  
8, 258, 259, 9, 8  
9, 259, 260, 10, 9  
10, 260, 261, 11, 10  
11, 261, 262, 12, 11  
12, 262, 263, 13, 12  
13, 263, 264, 14, 13  
14, 264, 265, 15, 14  
15, 265, 266, 16, 15  
16, 266, 267, 17, 16  
17, 267, 268, 18, 17  
18, 268, 269, 19, 18  
19, 269, 270, 20, 19  
20, 270, 271, 21, 20  
21, 271, 272, 22, 21  
22, 272, 273, 23, 22  
23, 273, 274, 24, 23  
24, 274, 275, 25, 24  
25, 275, 276, 26, 25  
26, 276, 277, 27, 26  
27, 277, 278, 28, 27  
28, 278, 279, 29, 28  
29, 279, 280, 30, 29  
30, 280, 281, 31, 30  
31, 281, 282, 32, 31  
32, 282, 283, 33, 32  
33, 283, 284, 34, 33  
34, 284, 285, 35, 34  
35, 285, 286, 36, 35  
36, 286, 287, 37, 36  
37, 287, 288, 38, 37  
38, 288, 289, 39, 38  
39, 289, 290, 40, 39  
40, 290, 291, 41, 40  
41, 291, 292, 42, 41  
42, 292, 293, 43, 42  
43, 293, 294, 44, 43  
44, 294, 295, 45, 44  
45, 295, 296, 46, 45  
46, 296, 297, 47, 46  
47, 297, 298, 48, 47  
48, 298, 299, 49, 48

```

49, 299, 300, 50, 49
50, 300, 301, 51, 50
.
.
.
60480, 60972, 60973, 60723, 60722
60481, 60973, 60974, 60724, 60723
60482, 60974, 60975, 60725, 60724
60483, 60975, 60976, 60726, 60725
60484, 60976, 60977, 60727, 60726
60485, 60977, 60978, 60728, 60727
60486, 60978, 60979, 60729, 60728
60487, 60979, 60980, 60730, 60729
60488, 60980, 60981, 60731, 60730
60489, 60981, 60982, 60732, 60731
60490, 60982, 60983, 60733, 60732
60491, 60983, 60984, 60734, 60733
60492, 60984, 60985, 60735, 60734
60493, 60985, 60986, 60736, 60735
60494, 60986, 60987, 60737, 60736
60495, 60987, 60988, 60738, 60737
60496, 60988, 60989, 60739, 60738
60497, 60989, 60990, 60740, 60739
60498, 60990, 60991, 60741, 60740
60499, 60991, 60992, 60742, 60741
60500, 60992, 60993, 60743, 60742
60501, 60993, 60994, 60744, 60743
60502, 60994, 60995, 60745, 60744
60503, 60995, 60996, 60746, 60745
60504, 60996, 60997, 60747, 60746
60505, 60997, 60998, 60748, 60747
60506, 60998, 60999, 60749, 60748
60507, 60999, 61000, 60750, 60749
*Elset, elset=LOW_FILM, generate
  701, 42330, 1
*Elset, elset=SUB, generate
  42331, 60507, 1
*Elset, elset=UP_FILM, generate
  1, 700, 1
** Section: Section-1-UP_FILM
*Solid Section, elset=UP_FILM, material=SN
,
** Section: Section-2-LOW_FILM
*Solid Section, elset=LOW_FILM, material=SN
,
** Section: Section-3-SUB
*Solid Section, elset=SUB, material=SN
,
*End Part
**
**
** ASSEMBLY
**
*Assembly, name=Assembly
**
*Instance, name=BSURF-1, part=BSURF
*Node
999999999, 0., 1.

```

```

*Nset, nset=BSURF-1-RefPt_, internal
999999999,
*Surface, type=SEGMENTS, name=BSURF-1-BSURF
START, 27.929, 10.
LINE, 0., 0.
*End Instance
**
*Instance, name=PART-1-1, part=PART-1
*End Instance
**
*Nset, nset=BOTTOM, instance=PART-1-1, generate
60751, 61000, 1
*Nset, nset=LEFT, instance=PART-1-1, generate
1, 60751, 250
*Nset, nset=N9999, instance=BSURF-1
999999999,
*Nset, nset=RIGHT, instance=PART-1-1, generate
250, 61000, 250
*Nset, nset=TOP, instance=PART-1-1, generate
1, 250, 1
*Elset, elset=SET-1, instance=PART-1-1, generate
1, 200, 1
*Elset, elset=WHOLE, instance=PART-1-1, generate
1, 60507, 1
*Elset, elset=__PICKEDSURF7_S3, internal, instance=PART-1-1, generate
1, 200, 1
*Nset, nset=_Ref-Pt_BSURF-1_999999999, internal, instance=BSURF-1
999999999,
*Elset, elset=_ASURF_S3, internal, instance=PART-1-1, generate
1, 200, 1
*Surface, type=ELEMENT, name=ASURF
_ASURF_S3, S3
** Constraint: RigidBody-1
*Rigid Body, ref node=_Ref-Pt_BSURF-1_999999999, analytical surface=BSURF-1.BSURF-1-BSURF
*End Assembly
**
** MATERIALS
**
*Material, name=SN
*Creep
1.24e-12, 7., 0., 20.
*Elastic
46000., 0.34
*Expansion
2.4e-05,
**
** INTERACTION PROPERTIES
**
*Surface Interaction, name=PAIRNAME
1.,
*Friction, slip tolerance=0.005
0.1,
**
** BOUNDARY CONDITIONS
**
** Name: Disp-BC-1 Type: Displacement/Rotation
*Boundary
LEFT, 1, 1

```

```

** Name: Disp-BC-2 Type: Displacement/Rotation
*Boundary
BOTTOM, 2, 2
** Name: Disp-BC-3 Type: Displacement/Rotation
*Boundary
N9999, 1, 1
** Name: Disp-BC-4 Type: Displacement/Rotation
*Boundary
N9999, 6, 6
**
** INTERACTIONS
**
** Interaction: PAIRNAME-1
*Contact Pair, interaction=PAIRNAME
ASURF, BSURF-1.BSURF-1-BSURF
** -----
**
** STEP: Step-1
**
*Step, name=Step-1, nlgeom=YES, amplitude=RAMP, inc=10000000, unsymm=YES
*Visco, cetol=5e-05
0.01, 10., 1e-09, 10.
**
** LOADS
**
** Name: CFORCE-1 Type: Concentrated force
*Cload, op=NEW
N9999, 2, -100.
**
** OUTPUT REQUESTS
**
*Restart, write, frequency=0
**
** FIELD OUTPUT: F-Output-1
**
*Output, field, variable=PRESELECT, frequency=100
**
** HISTORY OUTPUT: H-Output-7
**
*Output, history
*Node Output, nset=N9999
CF2,
**
** HISTORY OUTPUT: H-Output-8
**
*Node Output, nset=N9999
U2,
**
** HISTORY OUTPUT: H-Output-2
**
*Node Output, nset=TOP
COOR1, COOR2, COOR3
**
** HISTORY OUTPUT: H-Output-1
**
*Output, history, variable=PRESELECT
*End Step
** -----

```

```

**
** STEP: Step-2
**
*Step, name=Step-2, nlgeom=YES, amplitude=RAMP, inc=1000000, unsymm=YES
*Visco, ceto1=5e-05
0.01, 108000., 1e-07, 108000.
**
** LOADS
**
** Name: CFORCE-1 Type: Concentrated force
*Clod, op=NEW
** Name: CFORCE-2 Type: Concentrated force
*Clod, op=NEW
N9999, 2, -100.
**
** OUTPUT REQUESTS
**
*Restart, write, frequency=0
**
** FIELD OUTPUT: F-Output-2
**
*Output, field, variable=PRESELECT, frequency=200
**
** HISTORY OUTPUT: H-Output-7
**
*Output, history
*Node Output, nset=N9999
CF2,
**
** HISTORY OUTPUT: H-Output-8
**
*Node Output, nset=N9999
U2,
**
** HISTORY OUTPUT: H-Output-4
**
*Node Output, nset=TOP
COOR1, COOR2, COOR3
**
** HISTORY OUTPUT: H-Output-3
**
*Output, history, variable=PRESELECT
*End Step
** -----
**
** STEP: Step-3
**
*Step, name=Step-3, nlgeom=YES, amplitude=RAMP, inc=1000000, unsymm=YES
*Visco, ceto1=5e-05
0.01, 10., 1e-09, 10.
**
** LOADS
**
** Name: CFORCE-2 Type: Concentrated force
*Clod, op=NEW
**
** OUTPUT REQUESTS
**

```



```
*Restart, write, frequency=0
**
** FIELD OUTPUT: F-Output-3
**
*Output, field, variable=PRESELECT, frequency=200
**
** HISTORY OUTPUT: H-Output-7
**
*Output, history
*Node Output, nset=N9999
CF2,
**
** HISTORY OUTPUT: H-Output-8
**
*Node Output, nset=N9999
U2,
**
** HISTORY OUTPUT: H-Output-6
**
*Node Output, nset=TOP
COOR1, COOR2, COOR3
**
** HISTORY OUTPUT: H-Output-5
**
*Output, history, variable=PRESELECT
*End Step
```